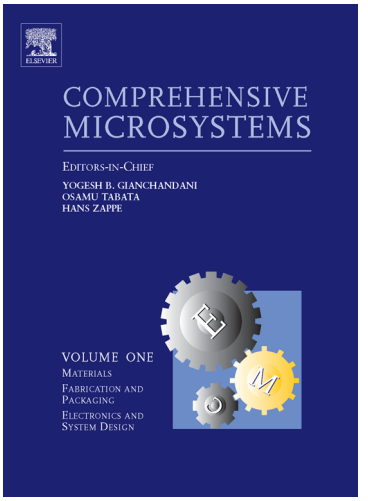

Karl Böhringer (2008), Self-Assembly. In: Yogesh B Gianchandani, Osamu Tabata, Hans Zappe, (Editors in Chief) Comprehensive Microsystems, Volume 1, pp. 403-430. Amsterdam: Elsevier.

1.14 Self-Assembly

Jiandong Fang and Karl F Böhringer, University of Washington, Seattle, WA, USA

1.14.1 Introduction and Motivation

1.14.1.1 The Growing Need for Assembly

Microassembly is a technique for producing complex microstructures and systems by integrating microcomponents made in separate manufacturing processes. Two-dimensional microassembly mounts components on a flat substrate, and 3D microassembly produces structures with a more intricate spatial geometry.

Both 2D and 3D microassemblies are needed for mass production of microdevices. For example, a radio frequency identification (RFID) tag consists of a silicon microchip and an antenna. The antenna powers the tag and exchanges data between the chip and a neighboring RFID reader. The key to efficient

Comprehensive Microsystems, vol. 1, pp.403-429

fabrication of RFID tags lies in the rapid replacement of the small, more expensive silicon microchips with the larger, cheaper antenna substrate (Silicon Chip Online 2006). Another example for a microassembly is smart dust, i.e., collections of tiny distributed nodes that integrate sensing capabilities with signal processing and can organize into a communications network (Warneke *et al.* 2001). These systems are emerging as commercial products, and microassembly techniques play a very important role in mass production of such microscale devices.

1.14.1.2 Monolithic Fabrication vs. Hybrid Integration

Monolithic fabrication constructs a whole device step by step from a single substrate. Hybrid integration constructs a device by combining various components from different techniques or processes. For devices with simple structures, monolithic fabrication has advantages such as compact layout and easy encapsulation. But many fabrication processes and materials are not compatible with one another, and thus microdevices having complex functionalities or structures must be constructed by hybrid integration of multiple units from several different fabrication processes.

Additionally, hybrid integration has another significant advantage for product developers. A complex microsystem can be broken down into multiple distinct units. Each unit is then assigned to a separate process engineer or group. Each unit can be separately optimized in design and fully characterized before integration. Units of the same type can be fabricated at the highest spatial density on a single substrate to save fabrication costs.

1.14.1.3 Packaging: Die Level vs. Wafer Level

Typically, packaging of microdevices involves three process steps:

(1) Placement of microdevices with correct face and in-plane orientations on receptor sites
(2) Permanent bonding of microdevices with electrical interconnections to the substrate
(3) Encapsulation of the bonded device components for protection from the environment

The choice of bonding method depends on the placement of microdevices: flip chip bonding is used for microdevices with electrical interconnects facing the substrate and wire bonding is used for microdevices with electrical interconnects facing the same direction as their counterparts on the substrate. A flip chip bonding process achieves electrical and mechanical connections simultaneously, and the electrical connections are established in parallel. A wire bonding process attaches a microdevice to the substrate to form mechanical connections before serial establishment of electrical connections. Die-level packaging assembles individual microcomponents after they are diced from a wafer. Wafer-level packaging simultaneously assembles all the devices on the same substrate before they are diced into individual devices, i.e., wafer-level packaging process is parallel assembly whereas die-level packaging is serial assembly.

1.14.2 State of the Art in Microassembly

1.14.2.1 Deterministic vs. Stochastic

Microassembly approaches, aimed at achieving highly efficient assembly of a very large number of microcomponents, can be classified into two major categories: deterministic and stochastic (**Figure 1**). In a deterministic assembly process, each part is assigned to a specific receptor site, e.g., as in wafer-to-wafer transfer of microstructures. In a stochastic assembly process, each part can be attached to any of the specifically designed identical receptor sites. The term self-assembly usually describes such stochastic assembly approaches, owing to the property that the assembly takes place in a spontaneous manner with components of a specific design. Self-assembly processes are discussed in detail in the remaining sections.

1.14.2.2 Serial vs. Parallel

The number of parts assembled at a time on a single platform defines the property of an assembly process: serial or parallel. In a serial assembly process, only one part is assembled at each time, for example, as in robotic pick-and-place assembly methods. In a parallel assembly process, multiple parts are assembled simultaneously, which can achieve a higher throughput. Both wafer-to-wafer transfer of microcomponents and self-assembly are parallel processes.

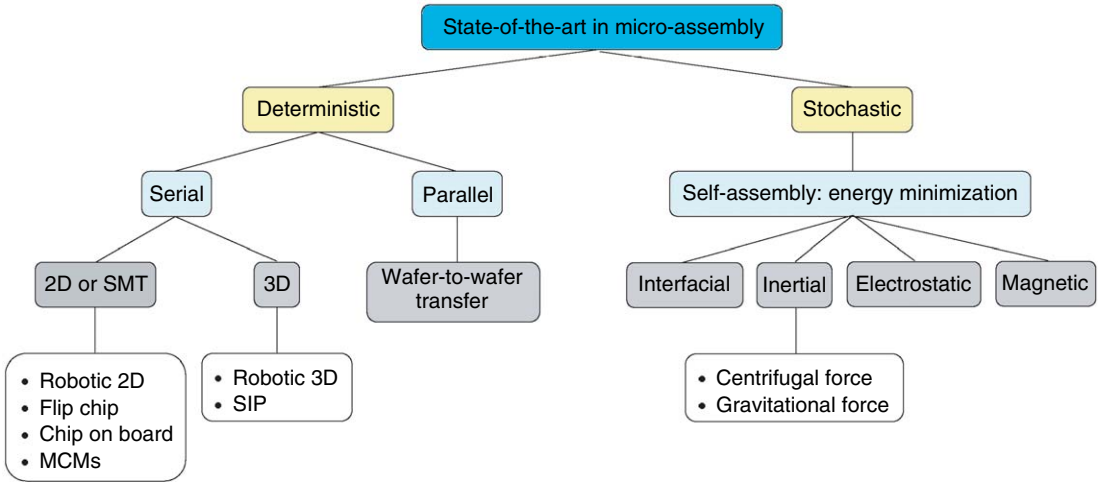

Figure 1 Categories of state-of-the-art microassembly techniques. MCM, multichip module; SIP, system in package.

1.14.2.3 Surface Mount vs. 3D Assembly

Surface mount technology (SMT) was fully established in the 1980s, when circuits became more and more complex so that through-hole component-mounting techniques were no longer economically or technologically feasible. The limitations in conventional printed circuit (PC) board technology motivated circuit design engineers to develop SMT. SMT keeps components and their interconnecting leads on one PC board surface, rather than feeding the component leads through the circuit board. SMT employs a solder to provide electrical and mechanical connections between components and PC boards. Compared with conventional through-hole mounting techniques, SMT possesses many prominent benefits such as reduced component size, increased circuit density, reduced PC board size, reduced weight, increased interconnecting leads density, and improved high-frequency performance. No single electronic assembly technology is perfect for satisfying all circuit design constraints. Current SMT also has some significant limitations such as poor heat dissipation, thermal mismatch, and decreased mechanical bonding strength of solder. SMT has a wide range of applications in packaging IC or microelectromechanical systems (MEMS) components, e.g., chip-on-board (COB) and multichip modules (MCMs).

Robotic assembly is a serial deterministic method widely used in industry to assemble a variety of components. This assembly approach has three major steps:

(1) Feed parts
(2) Pick and place parts
(3) Affix parts in specified position and orientation

During a typical part feeding step, randomly agitated components move through a series of mechanical filters so that finally they show appropriate face and in-plane orientations. Then robotic grippers pick up these components and transfer them to targeted sites to complete the assembly. This is a serial assembly process. Different part feeding mechanisms are required by various types (geometry or material fragility) of components. Zyvex Corporation has constructed small semiautomated robotic systems for microscopic and nanoscopic assemblies (Skidmore *et al.* 2000). Flat silicon microcomponents are a big challenge for part feeding since they are symmetrical except for negligible differences in geometric features on some surfaces, such as interconnecting pads. Depending on the degrees of freedom of the gripper, robotic assemblies can achieve 2D surface mount or 3D assembly.

A system in package (SIP) comprises multiple components integrated into a single package. In a typical SIP, components can be stacked vertically with 3D electrical interconnections; thus SIPs tend to be compact with much less parasitic capacitance and inductance.

1.14.3 Self-Assembly

Self-assembly techniques for component-to-substrate assembly are mainly based on energy minimization (**Figure 2**). A substrate is patterned with an array of energy traps. The types of energy traps include inertial, interfacial, electrostatic, and magnetic energies. On an assembly substrate, agitated

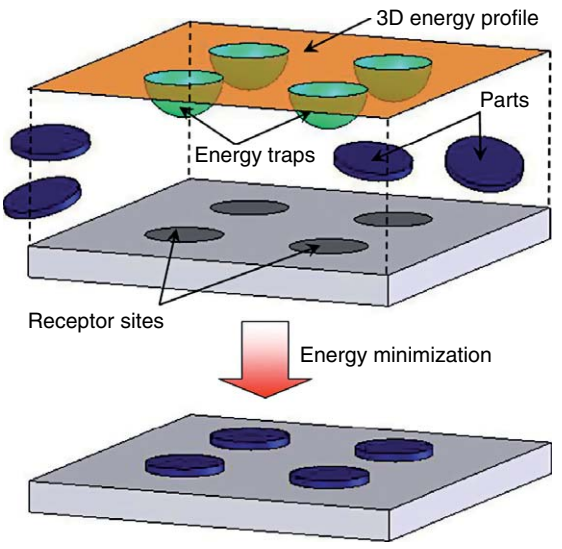

Figure 2 Schematic diagrams showing a typical self-assembly process based on energy minimization: on a substrate, patterned receptor sites are energy traps to attract the surrounding agitated microcomponents.

components are attracted to these energy traps and then permanently attached. Thus, components self-assemble to receptor trap sites on the substrate.

Compared with SMT and robotic pick-and-place assembly methods, self-assembly techniques have several major advantages such as easy handling of components with size in microdomains, fast parallel assembly, and self-alignment with high accuracy.

1.14.3.1 2D-Conformal-3D

A 2D conformal self-assembly process positions microcomponents on a rigid or flexible substrate, and the flat components attach directly to the substrate, i.e., assembled components are conformal with the substrate surface. This is the most common type of self-assembly, since patterning of energy traps on a substrate is straightforward with current microfabrication and surface modification techniques.

Three-dimensional self-assembly of microcomponents poses more challenges to currently available microfabrication techniques than does 2D self-assembly. Some simple 3D microstructures have been constructed by self-assembly processes based on shape matching and interfacial energy minimization (Gracias *et al.* 2000, Zheng *et al.* 2004), but this bottom-up fabrication method for complicated 3D microstructures still requires more breakthrough innovations in microfabrication techniques and assembly mechanisms.

1.14.3.2 Hard-Coded vs. Programmed

Depending on whether the probability for parts to attach to receptor sites can be adjusted by varying conditions, self-assembly processes can be categorized into hard-coded or programmed types. In a hard-coded assembly process, each receptor site has a constant probability to attach a part at any time. In a programmable assembly process, a receptor site has different affinities for a part under different conditions such as assembly environment and surface hydrophobicity, i.e., a receptor site can be turned on (an energy trap) or off (at the same energy level as its background or even higher). A typical usage of programmed self-assembly is to integrate different types of microcomponents on an array of receptor sites patterned by a single fabrication process.

1.14.3.3 Electrostatic and Electromagnetic Self-Assembly

1.14.3.3.1 Electrostatic 2D assembly

Electrostatic 2D assembly is based on the electrostatic attraction of microcomponents, and the electrostatic attraction is due to the polarization of the microcomponents in electrical fields. According to Coulomb's law, electrostatic force is inversely proportional to the square of the distance between charges, and thus it is a short-range interaction. Patterned surface areas with charges or localized electrical fields can be binding sites for microcomponents, and the binding strength increases with surface charge density or electrical field intensity.

Tien *et al.* (1997) exploited electrostatic interactions for direct patterning of 10-μm diameter gold disks on functionalized substrate surfaces. They fabricated the small charged gold disks by electroplating gold into photoresist molds and derivatizing these disks with charged self-assembled monolayers (SAMs), and patterned the planar or curved substrate with surface charges by microcontact printing or photolithography. By agitation, the charged gold disks aggregated on the regions with the opposite charges. Finally, they obtained selective and dense assembly in solutions such as methanol, ethanol, IPA, and dioxane (**Figure 3**).

Cohn *et al.* (1995) demonstrated a self-assembly process with alignment capabilities over electrostatic traps. The experiment was performed in an aqueous environment. The electrostatic traps were fabricated on a silicon substrate: a layer of 2-μm low-temperature oxide (LTO) was first deposited

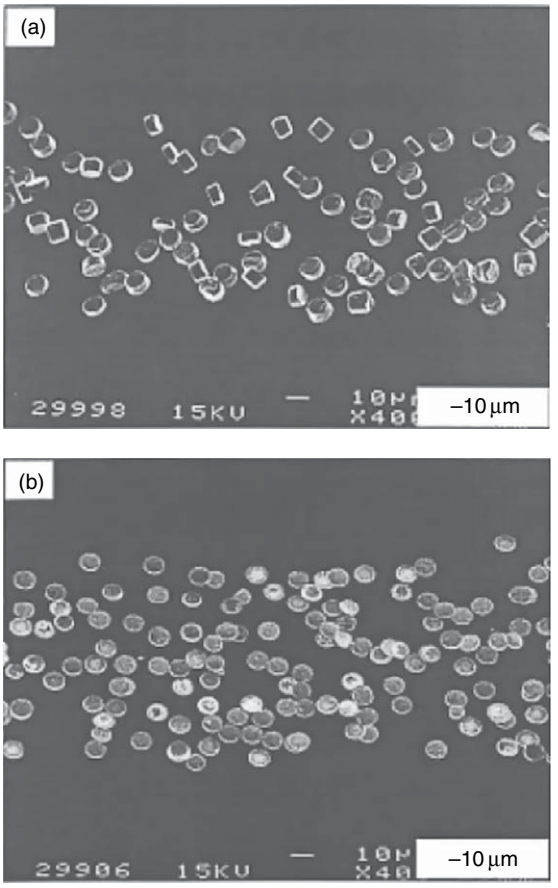

Figure 3 Scanning electron micrographs (SEMs) of PO_3H-terminated gold disks assembled on patterned gold. Gold wafers were patterned with HS-$(CH_2)_{15}$COOH and washed with 1 mM HS$(CH_2)_{11}NMe^{3+}$ and 1% HCl/EtOH. (a) Disks with an aspect ratio near 1:1 did not overlap each other. (b) Disks with an aspect ratio of 1:15 overlapped occasionally. (Photo courtesy: Tien J, Terfort A, Whitesides G M 1997 Microfabrication through electrostatic self-assembly. *Langmuir* **13**, 5349–55.)

as a dielectric layer by using low-pressure chemical vapor deposition (LPCVD), and then a layer of Au was deposited and patterned with an array of apertures (in the size ranges from 2 to 100 μm). The silicon substrate and the Au layer acted as two driving electrodes, which resulted in fringing electric fields from the patterned apertures in the Au layer. If the microcomponents stick to the substrate or to each other, there is no way to distribute or to assemble them to the specified binding sites or to the electrostatic traps on the substrate. They demonstrated a method to avoid such sticking phenomena by levitating the microcomponents a short distance (0–100 μm) above the target electrostatic traps before letting them settle, and thus accurate placement and orientation of the microcomponents with respect to the binding traps became feasible with a relatively low applied field of $\sim 10\,V\,\mu m^{-1}$. Each microcomponent (a SiO_2–*p*-Si–SiO_2 sandwich) had an average dielectric constant of 10, and the assembly liquid environment was hexane with a relatively low permittivity; therefore, microcomponents were easily attracted to the charged electrodes. The levitation of microcomponents was achieved by adding a small amount of a more polar solvent (acetone, with a relatively high dielectric constant of ~20), i.e., acetone shielded the electric field from the microcomponents and prevented contact of microcomponents with the binding sites. When all trap sites were occupied with floating microcomponents, the polar solvent was titrated out to lower the microcomponents to contact the trap sites. Finally, permanent bonding could be accomplished with sintering metals.

Fringing electric fields out of patterned apertures on a substrate can be exploited for assembling microparts in an air environment (Böhringer *et al.* 1998). The experimental setup is shown schematically in **Figure 4**. A glass substrate was coated with a layer of Cr/Au and the Cr/Au was patterned with an array of square holes to expose the glass underneath. The glass substrate was mounted on an aluminum vibratory platform driven by a piezoelectric actuator. Bulk parts were placed on the glass substrate. For effective agitation of these parts (initially parts tended to stick to the substrate and to each other because of the combination of electrostatic interaction and capillary and van der Waals forces), the vibrating frequency was chosen in the 20-kHz range. A DC voltage was applied on the aluminum platform and the Au electrode, and the resulting fringing electric field from the apertures in the upper electrode induced polarization in neutral parts and caused them to be attracted to the apertures. When a part covered an upper electrode aperture, the fringing electric field was significantly reduced, which prevented attraction of more parts to this occupied site. Assembly experiments were performed in both air and low vacuum, and the results indicated that the vibrating energy required to overcome adhesive forces decreased with air pressure, probably due to squeeze film effects (Fearing 1995) and due to the vacuum created between the flat-part bottom surface and the substrate when operated at ultrasonic frequencies.

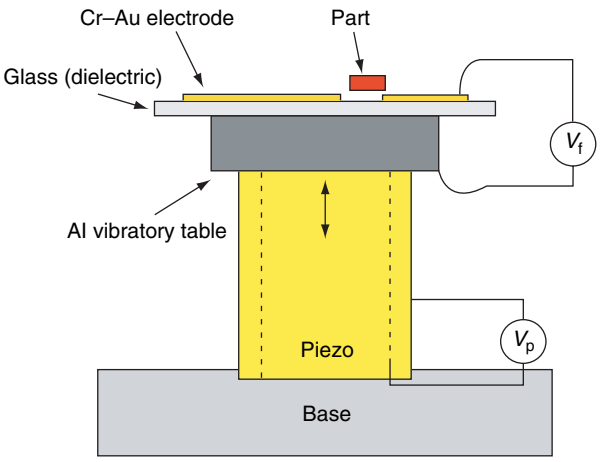

Figure 4 Schematic experimental setup for self-assembly with electrostatic traps: a vibratory table with a gold-covered dielectric is attached to a piezoelectric actuator. The aperture in the upper electrode creates a fringing field that causes polarization in the part. The part is attracted to the aperture. (Source: Böhringer, K F, Goldberg K, Cohn M, Howe R T, Pisano A 1998 Parallel microassembly with electrostatic force fields. *Proc. Int. Conf. Robotics and Automation (ICRA)*, Leuven, Belgium, pp. 1204–11.)

1.14.3.3.2 Toward 3D by triboelectricity

Kaajakari and Lal (2001) demonstrated a method based on triboelectricity for batch assembly of polysilicon hinged structures (**Figure 5**). Triboelectricity on hinged plates and the substrate was achieved by use of ultrasonic vibrations generated with an attached piezoelectric actuator to vibrate polysilicon plates on silicon nitride or polysilicon substrate surfaces. Such contact electrification charges resulted in hinged flaps being stabilized vertically on the substrate. Furthermore, they also observed a memory effect in which assembly occurred even without further ultrasonic vibration after the initial ultrasonic assembly.

1.14.3.3.3 Magnetic assembly

Magnetic force is a type of short-range interaction, and it can be utilized to attach microcomponents to magnetized sites on a substrate. Perkins *et al.* (2002) developed a new assembly approach called magnetically assisted statistical assembly (MASA): the compound semiconductor device heterostructures, 'nanopills' covered with a soft magnetic material, were trapped in the shallow recesses patterned into the surface of an integrated circuit wafer, and the short-range magnetic attractive forces kept the parts in the recesses (**Figure 6**). The 'nanopills' were agitated by liquid flow. **Figure 7** shows the

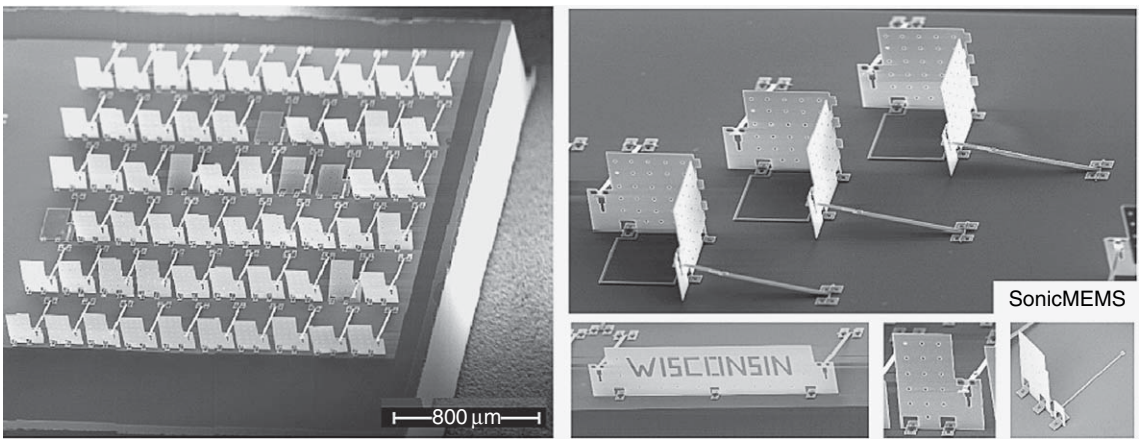

Figure 5 Examples of devices assembled with triboelectricity: array of assembled micromachined flaps, polysilicon corner cube reflectors (200 μm × 200 μm) with lock-in structure, and micro-art Wisconsin banner. Lower right shows a flap with a retaining spring latch anchored to the substrate. (Photo courtesy: Kaajakari V, Lal A 2001 Electrostatic batch assembly of surface MEMS using ultrasonic triboelectricity. *14th IEEE Int. Conf. Micro Electro Mechanical Systems*, pp. 10–13.)

relationship between the magnetic force per unit area and the separation between a part's permalloy surface and the magnetized Co–Pt stripes at the bottom of a recess.

Magnetic fields can also be exploited to construct 3D microstructures. Iwase *et al.* demonstrated a sequential batch assembly method (Iwase and Shimoyama 2005) based on the magnetic field-assisted self-assembly (**Figure 8**): an external magnetic field perpendicular to the substrate was used to lift the hinged ferromagnetic microstructures, and the magnetic field was increased gradually so that the plate with softer hinges was lifted first. The softness of a plate's hinge can be controlled by adjusting the length and the number of hinge beams.

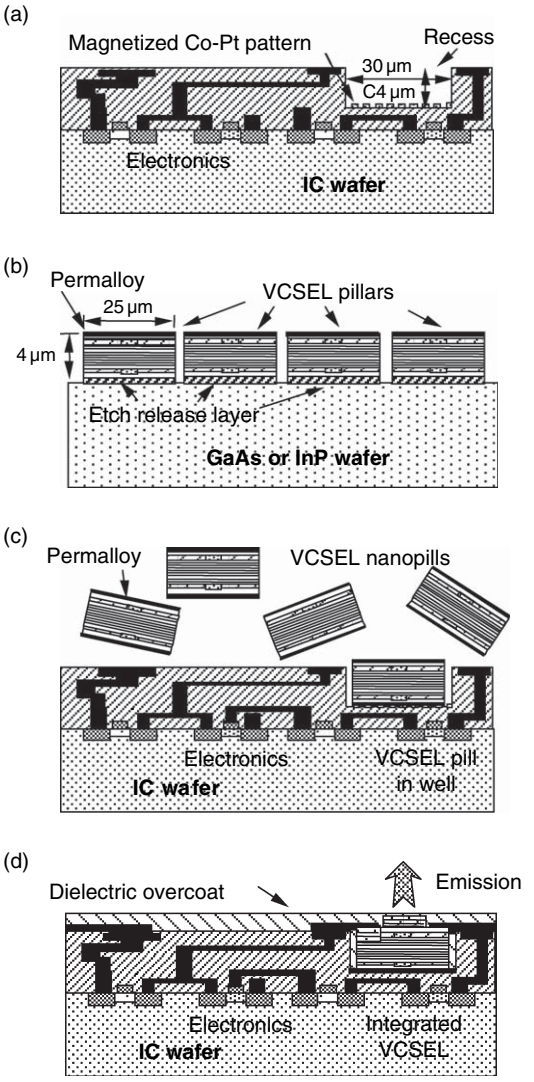

Figure 6 A schematic overview of the magnetically assisted statistical assembly (MASA) process: (a) the processed IC wafer with the recesses prepared; (b) the p-side down device wafer (in this case vertical cavity surface-emitting laser (VCSELs)) with pillars etched in a close-packed array; (c) stochastic assembly of the freed nanopills in the recesses on the IC wafer; (d) after completing device processing and integration. (Photo courtesy: Perkins J, Rumpler J, Fonstad C G 2002 Magnetically assisted self-assembly – A new heterogeneous integration technique. *MIT Microsystems Technology Laboratories Annual Report*.)

1.14.3.4 Shape Matching

1.14.3.4.1 Fluidic self-assembly

Fluidic self-assembly relies on shape matching between microcomponents and recessed receptor sites (Yeh and Smith 1994). Bulk microcomponents are agitated by liquid flow until they fall into receptor holes. GaAs vertical cavity surface-emitting laser (VCSEL) components were demonstrated to be integrated on a silicon substrate. The silicon host substrate was patterned with etched holes of trapezoidal shape, and the GaAs light-emitting diode (LED) components were also of the same trapezoidal shape. Carrier fluid containing the GaAs microcomponents was dispensed over the host silicon substrate. Because of the trapezoidal shape design, the GaAs blocks fit preferentially into the holes in the desired face orientation. Random mechanical vibration was performed to enable the precise positioning of a large number of microparts in the recessed receptor sites. More than 90% of the etched holes on the substrate were correctly filled with the GaAs blocks before the carrier fluid evaporated.

Alien Technology Corporation has commercialized this fluidic self-assembly technique (**Figure 9**). Fluidic self-assembly can work on either rigid (glass or plastic) or flexible (polyester, polyimide, polycarbonate, etc.) substrates. They have been using fully automated in-line reel-to-reel (web) processing on a continuous flexible substrate. Fluidic self-assembly and web processing offer many advantages over conventional processing on rigid substrates, such as those given below:

(1) Reduced manufacturing facility investment
(2) Reduced material and manufacturing costs
(3) Increased manufacturing throughput

Stauth *et al.* also used a fluidic self-assembly technique to integrate silicon microcomponents on a plastic substrate (Stauth and Parviz 2005). Receptor

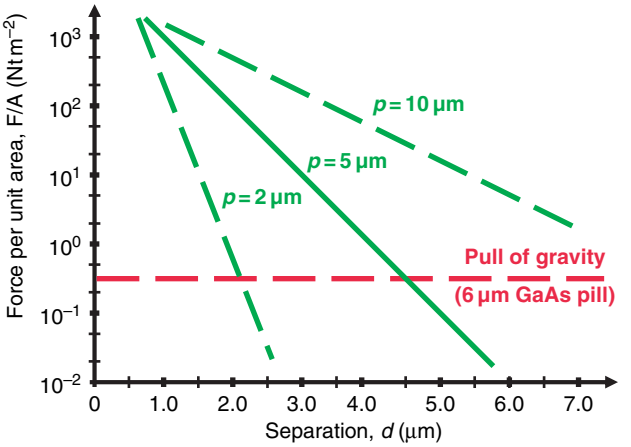

Figure 7 The attractive magnetic force per unit area as a function of separation for various spatial periods p of magnetic stripes at the bottom of the recesses. For comparison the pull of gravity on a 6-μm-thick GaAs nanopill is shown by the horizontal dashed line. (Photo courtesy: Perkins J, Rumpler J, Fonstad C G 2002 Magnetically assisted self-assembly – A new heterogeneous integration technique. *MIT Microsystems Technology Laboratories Annual Report*.)

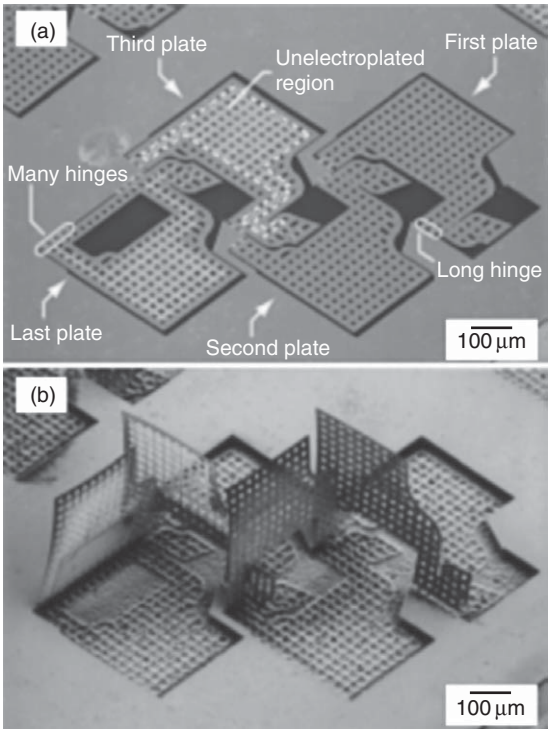

Figure 8 Scanning electron micrograph (SEM) of four-step sequential batch assembly driven by magnetic field: (a) before assembly; (b) after assembly. (Photo courtesy: Iwase E, Shimoyama I 2005 Multi-step sequential batch self-assembly of three-dimensional micro-structures using magnetic field. *Proc. IEEE Int. Conf. Micro Electromechanical Systems*, pp. 588–91.)

wells on the plastic substrate were formed with a lithographically patterned thick SU8. At the bottom of these receptor wells, electrical terminals were coated with low-temperature melting solder. Interconnect pads on silicon microcomponents are patterned Au areas with high solder-wetting capability. In a hot and acidic aqueous environment, microcomponents slid on the tilted substrate and fell into receptor wells, and then the microcomponents were anchored when their interconnect Au pads contacted melting solder droplets in the wells.

1.14.3.4.2 Dry self-assembly

Shape matching can also take place in a dry assembly environment such as air or vacuum. Dry assembly environments avoid potential physical damage to or chemical erosion of microcomponents. Fragile structures on a microcomponent, for example, cantilever beams, can be easily immobilized or even broken by surface tension forces of liquid residue from a wet assembly environment. Dry self-assembly techniques based on shape matching are discussed in Section 1.14.3.7.

1.14.3.5 Centrifugal Force-Driven Self-Assembly and toward 3D

For microscale components, inertial forces, for example, gravity, are usually neglected when compared with surface forces such as surface tension and electrostatic forces. As an inertial force, a centrifugal force can be increased to overcome surface forces because it is proportional to the square of the rotating speed.

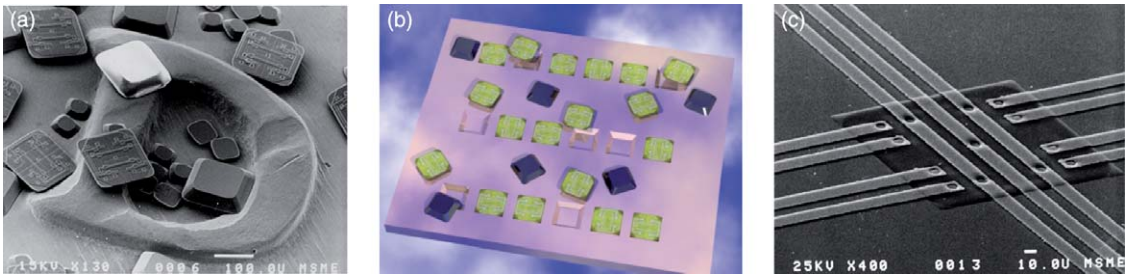

Figure 9 Fluidic self-assembly technique commercialized by Alien Technology: (a) microphotograph of individual nanoblocks on the surface of a dime; (b) artist's rendition of nanoblocks falling into substrate holes; (c) microphotograph of a passivated metallized nanoblock. (Photo courtesy: Alien Technology whitepaper published in 1999.)

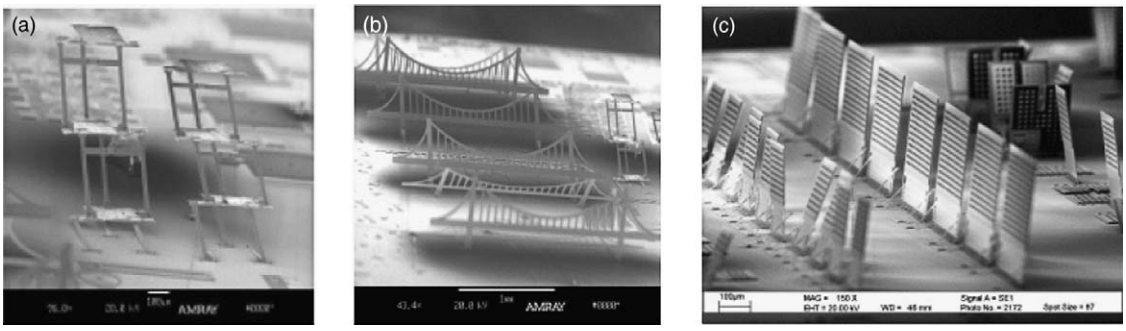

Figure 10 Microstructures assembled by centrifugal force: (a) tri-level poly-tower; (b) an array of Tsing-ma Bridge (a famous bridge in Hong Kong) structures; and (c) an array of microplates. (Photo courtesy: Lai K W C, Hui A P, Li W J 2002 Non-contact batch micro-assembly by centrifugal force. *Proc. IEEE Conf. Micro Electro Mechanical System*, pp. 184–7.)

Lai *et al.* (2002) demonstrated noncontact batch assembly of 3D microstructures by centrifugal force. Hinged microstructures fabricated in a multi-user MEMS process (MUMPs) were assembled with the help of latching features by centrifugal forces (**Figure 10**).

1.14.3.6 Capillary Self-Assembly

1.14.3.6.1 Toward 3D with solder/photoresist reflow

In microdomains, surface tension forces dominate over gravitational forces, and they have been explored and exploited by some researchers to lift hinged plates for constructing 3D structures (Syms *et al.* 2003). To achieve this type of 3D assembly, a thick layer of solder or photoresist is usually deposited and patterned at the joint of hinged structures. When the solder or photoresist is reflown, it changes into a spherical shape to minimize interfacial energies (a spherical shape has the minimum surface-to-volume ratio), and thus the hinged plate attached to the reflowed droplet rotates. With appropriate latching features, some complex 3D microstructures can be constructed (**Figure 11**).

Yang *et al.* (2006) developed a method to achieve local assembly by reflowing solder with magnetic induction welding. The heating temperature depends on the area of the magnetic film underneath the solder, and thus different heating temperature regions on a substrate can be photolithographically defined (the magnetic field is assumed to be uniform across the substrate). They demonstrated this technique by separating Ni plates from Ti plates (**Figure 12**).

Zheng *et al.* (2004) used a low-temperature melting solder to construct functional circuits that consisted of 3D structures including a LED component, a chip carrier with solder bumps, and an encapsulation body with solder bumps. The assembly sequence was as follows (**Figure 13**):

(1) LED components and chip carrier components were put in a hot and acidic liquid environment, where tumbling agitation caused each LED component to attach to a chip carrier component. Finally, the attached components with the solder bonding were sorted out.

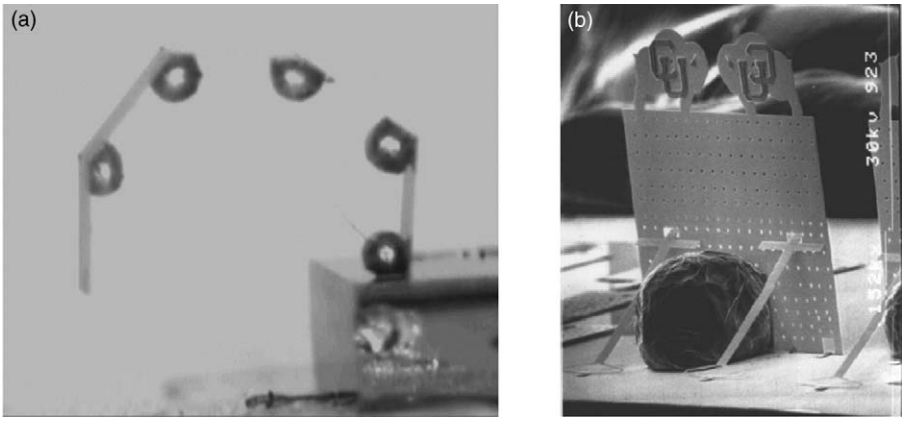

Figure 11 Optical graphs of some 3D self-assembled structures by reflowed solder: (a) 5-bar multiple link assembly. (Photo courtesy: Harsh K F, Kladitis P E, Zhang Y H, Dunn M L, Bright V M, Lee Y C 2000 Tolerance and precision study for solder self-assembled MEMS. *Proc. SPIE* **4075**, 173–84.) (b) A flap vertically assembled. (Photo courtesy: Kladitis P E, Bright V M 2000 Prototype microrobots for micro-positioning and micro-unmanned vehicles. *Sens. Actuators* **A80**, 132–7.)

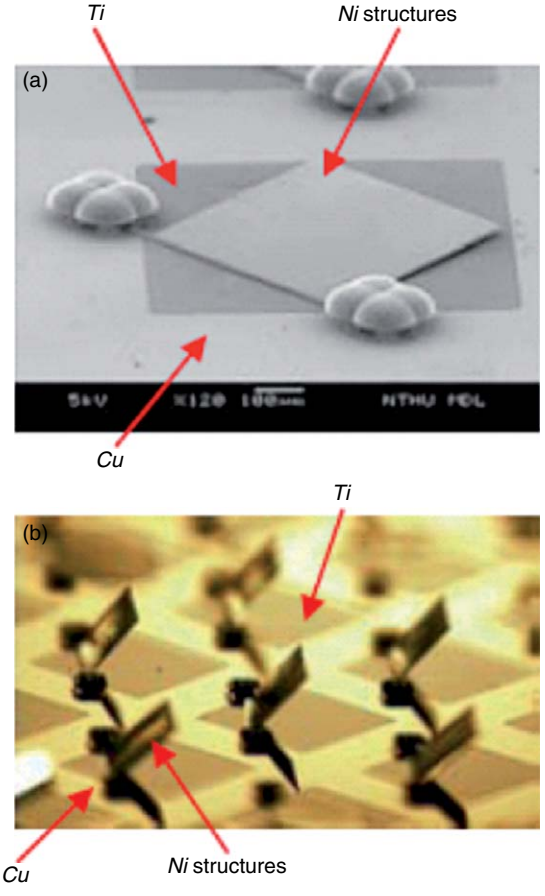

Figure 12 Optical micrographs of the tested structure to show separation of Ni and Ti films: (a) before and (b) after applying magnetic field. (Photo courtesy: Yang H, Lin C, Fang W 2006 Wafer level self-assembly of microstructures using global magnetic lifting and localized induction welding. *IOP J. Micromech. Microeng.* **16**, 27–32.)

(2) The attached components from the previous step were placed in a hot and acidic liquid environment together with encapsulation components for another batch assembly.

1.14.3.6.2 Parallel 2D assembly

In capillary-driven 2D self-assembly processes, agitated flat microcomponents contact and attach to adhesive liquid droplets on receptor sites, and then self-align to receptor sites to minimize interfacial energies. Depending on the assembly environment, capillary-driven self-assembly processes can be classified into two types: in an aqueous environment and in an air environment. Different adhesive liquids require different hydrophilicity or surface coatings for the receptor sites. For an acrylate-based adhesive liquid, receptor sites should be hydrophobic for aqueous assembly environments and hydrophilic for air assembly environments (**Figure 14**). For low-temperature melting solder, receptor sites should be thin film metals with good solder-wetting capability, e.g., copper and gold.

Low-temperature melting solder can be used to assemble flat microcomponents with both electrical and mechanical connections on a substrate. Jacobs *et al.* (2002) developed a self-assembly process to mount LED arrays on flexible cylindrical templates by using a low-temperature melting solder. The assembly template was patterned with copper squares, and a simple dip coating process left melting solder on these copper squares since copper has very good wetting capability for solder. The dip coating process was performed in an acidic aqueous

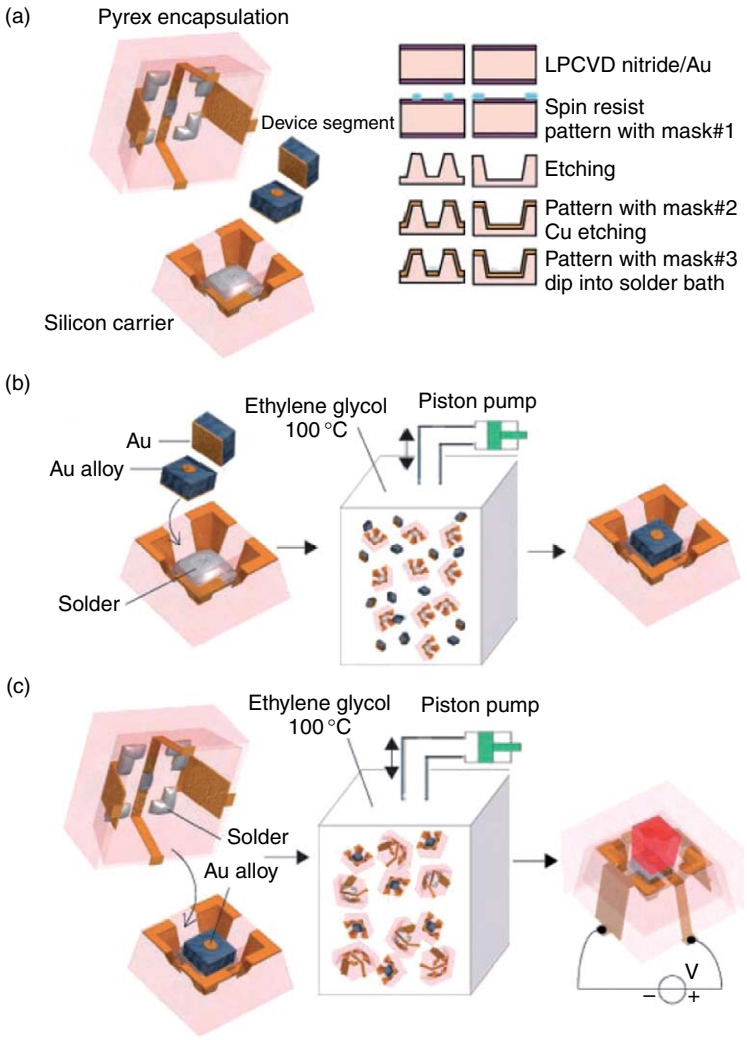

Figure 13 Schematic overview of the solder-directed 3D assembly of LED components. (a) Layouts of carrier, device, and encapsulation components fabricated by surface micromachining and etching. The illustrated device segment is a LED that has two contacts: a small circular anode on the front, and a large square cathode covering the back. The silicon carrier has a solder-coated area in a tapered opening to host a single semiconductor device segment. The encapsulation unit has five solder-coated copper areas inside a tapered opening to connect to corresponding contact pads on the device and the carrier. (b) Chip-on-carrier assembly and (c) chip encapsulation in an ethylene glycol solution at 100 °C, where the solder is melted. The components, agitated by using a piston pump, self-assemble and form a 3D circuit path between device layers that allows testing in a surface mount device configuration. (Photo courtesy: Zheng W, Buhlmann P, Jacobs H O 2004 Sequential shape-and-solder-directed self-assembly of functional microsystems. *Proc. Natl. Acad. Sci. USA* **101**, 12814–17.)

environment to avoid oxidation of the melting solder. Since a LED segment has electrical polarity, i.e., it can be lit only with an appropriate positive DC bias, two electrodes on either side of each LED segment should be distinguished with some pattern: the gold covered the whole bottom surface and 1/9th of the top surface. Hundreds of LED components and a flexible assembly template were placed inside a vial filled with water at a temperature above the melting point of the solder. The LED components were tumbled inside the vial, and then they were attracted, aligned, and bonded to the receptor sites on the template by the surface tension forces of the melting solder. By controlling the agitation intensity, only the bottom surfaces 100% covered gold instead of the top surface with 1/9 covered gold were bonded to solder droplets because the adhesion is roughly proportional to the gold-covering area on the LED segments. Therefore, the LED components self-assembled with unique face orientations. Gold pads

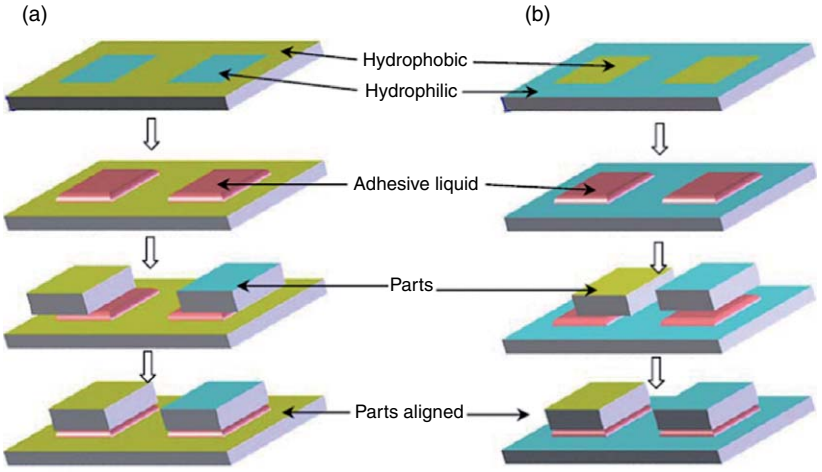

Figure 14 Schematic process overviews of capillary-driven self-assembly of flat microcomponents: (a) in an aqueous environment and (b) in an air environment.

on the top surfaces of the bonded LED components were coated with melting solder by another dip coating. As a final assembly step, a flexible transparent film patterned with electrical circuits and solder bumps was roughly and manually aligned to the assembly template, i.e., a wafer-level flip chip bonding process, and the film was aligned with high accuracy to the assembly template by surface tension of the melting solder. Thus, the electrical connections to the top electrodes of the LED segments were established. Assembly was successful by testing with a low defect rate of ~2% (**Figure 15**).

Srinivasan *et al.* (2001) developed and demonstrated another fluidic self-assembly technique. They patterned a substrate with an array of hydrophobic thiolated Au binding sites. When the substrate was inserted into water through a film of hydrophobic adhesive floating on the water surface, the adhesive covered only the hydrophobic binding sites. Then they introduced microparts fabricated from silicon-on-insulator wafers through a pipette to the substrate in the water. When the hydrophobic pattern on the microparts came in contact with the adhesive, shape matching occurred spontaneously due to interfacial energy minimization. Finally, the adhesive was polymerized by heat or UV light depending on the type of the adhesive, so that the bonding became permanent. Binding sites of shapes with in-plane rotational symmetries such as squares gave alignment yields up to 100% (**Figure 16(a)**). The translational and rotational misalignments were <0.2 μm and within ~0.3°, respectively. Binding sites without in-plane rotational symmetries (aimed at a

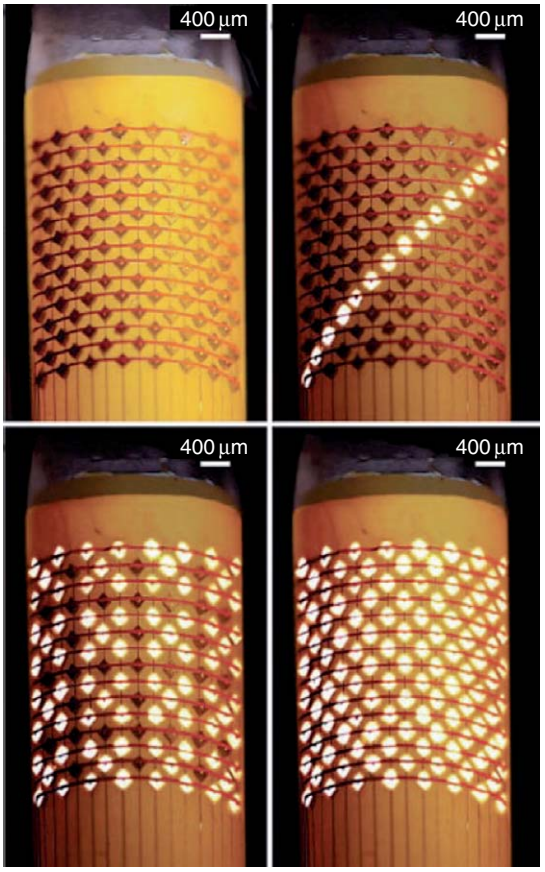

Figure 15 Optical photographs of tested light-emitting diode (LED) arrays self-assembled on a flexible substrate by capillary forces from low-temperature melting solder. (Photo courtesy: Jacobs H O, Tao A R, Schwartz A, Gracias D H, Whitesides G M 2002 Fabrication of cylindrical display by patterned assembly. *Science* **296**, 323–5.)

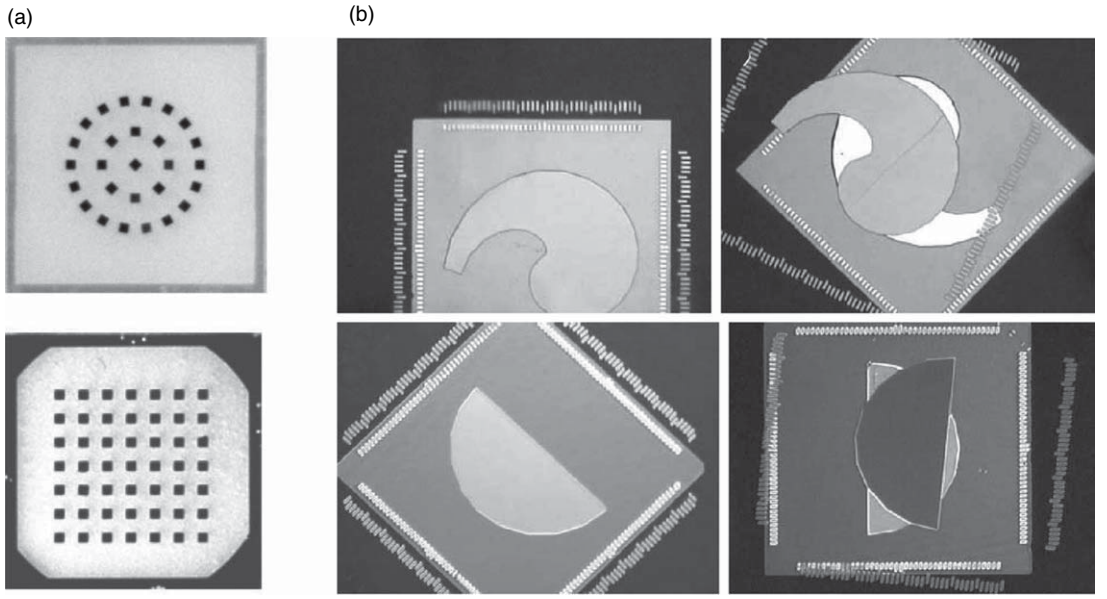

Figure 16 Optical micrographs of capillary-driven self-assembly of flat microparts: (a) square parts on quartz substrates in ring and grid configurations and (b) correct and wrong alignments for semicircle- and comma-shaped binding sites. (Source: Srinivasan U, Liepmann D, Howe R T 2001 Microstructure to substrate self-assembly using capillary forces. *J. Microelectromech. Syst.* **10**, 17–24.)

uniquely oriented alignment) such as semicircles and commas gave alignment yields of approximately 30–40% (**Figure 16(b)**).

To achieve self-assembly with unique in-plane orientations, Liang *et al.* (2004) designed and demonstrated a capillary-driven self-assembly process with special geometrical designs for binding sites. Both the parts and the binding sites are of an offset ring shape, which provides a unique global interfacial energy minimum (**Figure 17**): the energy calculation is based on the assumption that the interfacial energy has an approximately linear relationship with the overlap area between a part and the binding site (Böhringer *et al.* 2001).

Capillary-driven self-assembly can also proceed in an air environment as long as the receptor sites are coated with liquid droplets that act as a medium to attach flat microcomponents. Fang *et al.* (2006) have demonstrated a capillary-driven self-assembly method to surface mount PZT (lead zirconate titanate) actuators for microfluidic devices. The hydrophilic receptor sites are precisely recessed wells with an opening smaller than the PZT actuators, and the bonding face of each PZT actuator has a hydrophilic area of identical size at the center as the recess's opening. All the surfaces except the receptor wells and the bonding areas on the PZT actuators are hydrophobic. A simple dip coating process left adhesive droplets only in receptor wells. When PZT actuators were attached to these adhesive droplets, they self-aligned to minimize interfacial energies. Then, the aligned PZT actuators were pressed down such that their rims touched the substrate with excess adhesive squeezed out, and the electrically insulated adhesive was polymerized by heating to form permanent bonds. Electrical and mechanical connections were established at the rim and at the center, respectively, of the PZT actuators.

To introduce bulk microcomponents to receptor sites during dry assembly, Liang *et al.* (2005) developed a method using an agitated diaphragm to bounce microcomponents until some were caught by water droplets on the receptor sites on the downward-facing assembly substrate (**Figure 18**). This process demonstrated fast assembly (<30 s) and high yields (>90%), and fast recycling of redundant components. The glass substrate was coated with hydrophobic thiolated Au, which was patterned with an array of openings (exposure of the glass substrate). The exposed glass receptor sites were hydrophilic and covered with water droplets after a dip coating process. The capillary-driven alignment was a subsecond process (**Figure 19**).

1.14.3.6.3 Multibatch assembly

Xiong *et al.* demonstrated a method for controlled multibatch self-assembly, based on the fluidic self-assembly technique developed by Srinivasan *et al.*, of microparts by capillary force. They patterned an

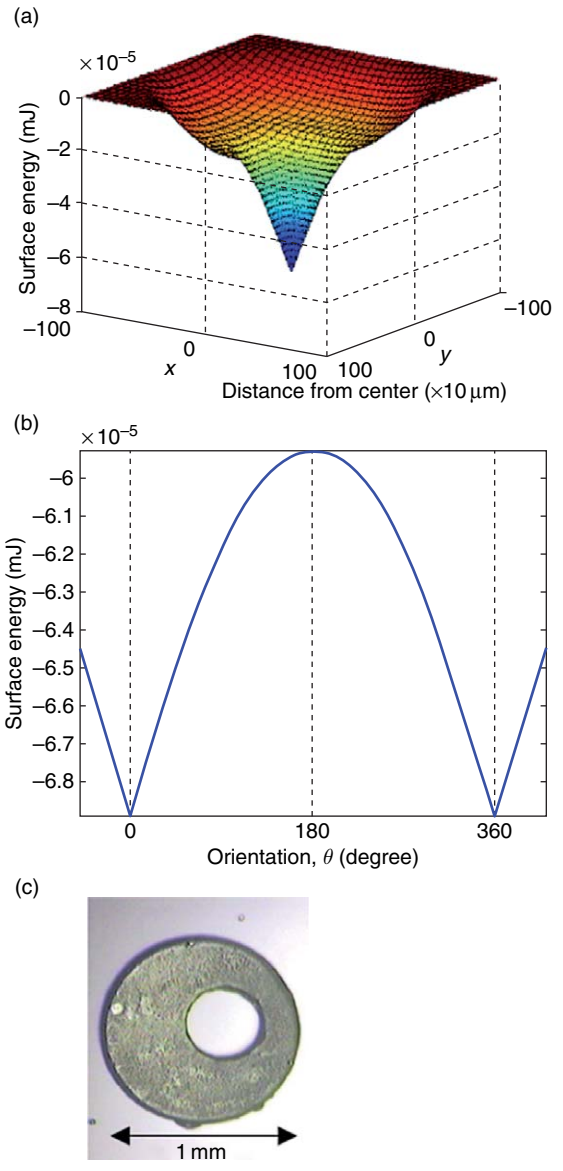

Figure 17 Energy profiles for an offset ring design: (a) the part with the correct in-plane orientation moves in a translational way across the binding site; (b) the part rotates about its center, which coincides with the binding site's center; and (c) an experimental result shows exact alignment of the silicon part over the thiolated gold binding site in water. (Photo courtesy: Liang S, Xiong X, Böhringer K F 2004 Towards optimal designs for self-alignment in surface-tension driven micro-assembly. *Proc. IEEE Conf. Micro Electro Mechanical Systems (MEMS)*, Maastricht, The Netherlands, pp. 9–12.)

oxidized silicon substrate with an array of gold binding sites, and these hydrophilic gold binding sites became hydrophobic after adsorbing a SAM. To be active, i.e., to adsorb an adhesive lubricant droplet for later

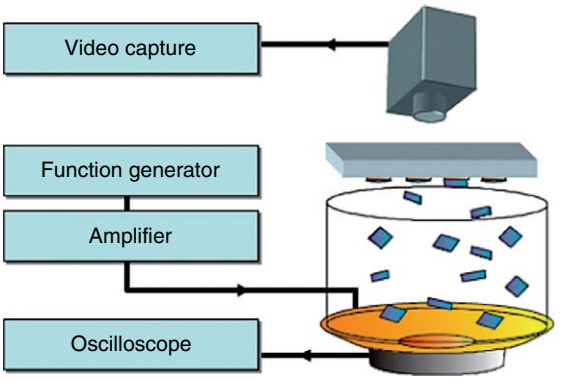

Figure 18 Schematic experimental setup: a sinusoidal wave signal from a function generator drives the speaker diaphragm to bounce microcomponents up until they make contact with the binding sites of the downward-facing assembly substrate. (Photo courtesy: Liang S, Wang K, Böhringer K F 2005 Self-assembly of MEMS components in air assisted by diaphragm agitation. *Proc. IEEE Conf. Micro Electro Mechanical Systems*, pp. 592–5.)

anchoring of parts, a binding site should be hydrophobic. They demonstrated an electrochemical method to desorb the SAM from the gold binding sites: an appropriate electrochemical potential was applied between the gold binding sites and an aqueous environment. Before the first batch assembly, some binding sites were selectively deactivated by SAM desorption, to be reactivated for the next batch assembly. An array of commercial LED components was assembled on the substrate with the heat polymerizable adhesive, and the electrical connections between the substrate and the LED components were established by solder electroplating (**Figure 20**).

1.14.3.7 Multistage Self-Assembly

1.14.3.7.1 Semidry, uniquely orienting, self-organizing parallel assembly

Fang and Böhringer have developed a semi-DUO-SPASS (dry, uniquely orienting, self-organizing parallel assembly) process for batch assembly of flat microcomponents. This semidry assembly process, based on the assembly strategy shown in **Figure 21**, includes two wet process steps followed by two dry process steps.

The parts used in demonstration were dummy flat silicon components with dimensions of 2 mm × 2 mm × 0.5 mm. Each part had a circular peg (ϕ 0.3 mm) located offset from the center of mass. The part surface opposite to the peg was the only hydrophobic face coated with thiolated gold (**Figure 22(a)**). Correspondingly, each

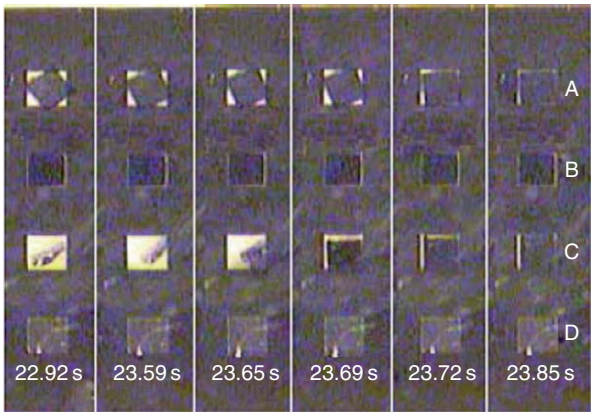

Figure 19 Video frames of one column of a receptor site array from an assembly experiment: A, alignment driven by surface tension; B and D, correctly aligned components; C, vertical attachment corrected by impacts. (Photo courtesy: Liang S, Wang K, Böhringer K F 2005 Self-assembly of MEMS components in air assisted by diaphragm agitation. *Proc. IEEE Conf. Micro Electro Mechanical Systems*, pp. 592–5.)

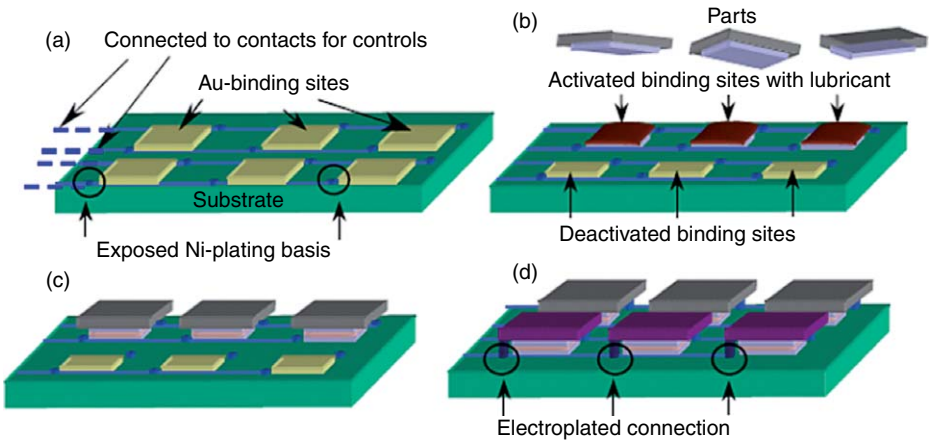

Figure 20 Multibatch assembly schematic flow: (a) A fabricated substrate for assembly with Au binding sites and Ni-plating basis. (b) A substrate prepared for first batch assembly. The substrate is immersed in water with lubricant wetting exclusively the activated binding sites. (c) First batch assembly. (d) By repeating the assembly process, the second batch of components is assembled. Electroplating is performed afterward to establish electrical interconnections. (Photo courtesy: Xiong X, Hanein Y, Fang J, Wang Y, Wang W, Schwartz D T, Böhringer K F 2003 Controlled multi-batch self-assembly of micro devices. *IEEE J. Microelectromech. Syst.* **12**, 117–27.)

receptor site on an assembly substrate had a circular well with a large diameter for easy adoption of a peg, but the well's diameter should have an upper limit to ensure that one well adopts exactly one peg (**Figure 22(b)**).

The first wet process step is to uniquely face-orient bulk silicon parts. An agitated water surface was exploited to selectively float silicon components with only their hydrophobic faces upward. For floating parts, the other two poses, horizontal with the hydrophilic face upward and vertical, are not stable due to surface tension forces. It was observed that the uniquely face-oriented floating parts stayed together in a single layer after agitation was turned off for several minutes, and this monolayer assembly phenomenon is driven by potential energy minimization.

A hydrophobic carrier wafer was employed to transfer the uniquely face-oriented floating parts. When the hydrophobic carrier wafer entered water vertically, the water surface curved downward near the hydrophobic surface to approach a contact angle $>90^\circ$. Such downward-curving surface resulted in a water valley near the carrier wafer surface, and this valley attracted the nearby floating

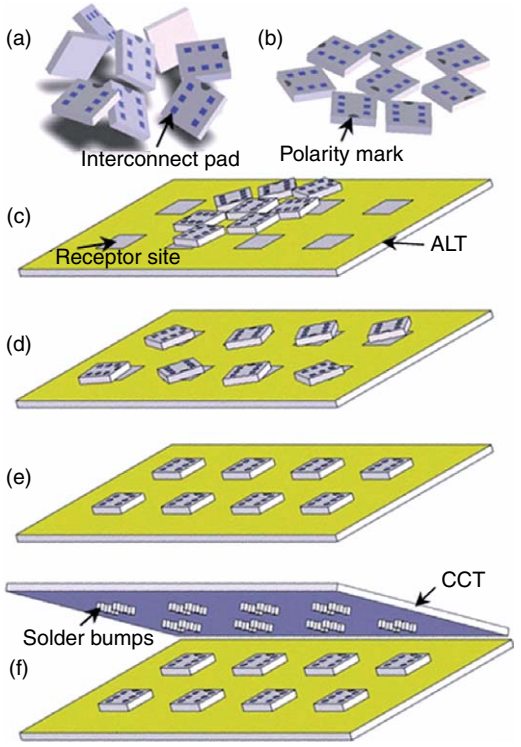

Figure 21 Batch assembly strategy: (a) randomly oriented bulk parts; (b) bulk parts are uniquely face-oriented and spread in a single layer; (c) parts are palletized on an alignment template; (d) parts are distributed one-to-one to receptor sites; (e) parts are aligned to the receptor sites with unique in-plane orientations; and (f) parts are bonded to a chip carrier template (CCT) via wafer-level flip chip bonding. (Source: Fang J, Böhringer K F 2006 Wafer-level packaging based on uniquely orienting self-assembly (the DUO-SPASS processes). *ASME/IEEE J. Microelectromech. Syst.* **15**, 531–40.)

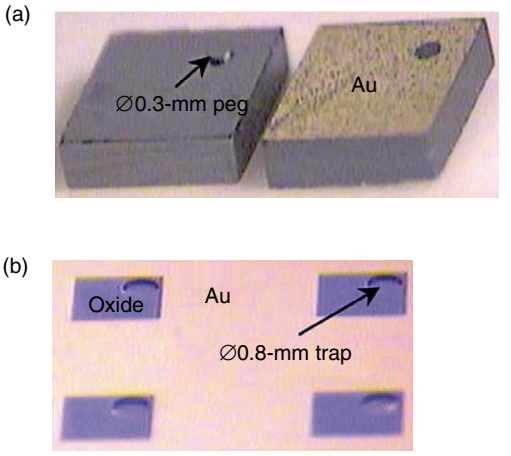

Figure 22 Microscope images of parts and receptor sites: (a) top and bottom views of 2-mm square silicon parts; (b) a 2×2 section of an array of 2-mm square receptor sites on a 4-in. alignment template. (Source: Fang J, Böhringer K F 2005 High yield batch packaging of micro devices with uniquely orienting self-assembly. *Proc. IEEE Conf. Micro Electro Mechanical Systems*, Miami, FL, USA, pp. 12–15.)

parts to minimize their potential energies (**Figure 23(a)**). As the carrier wafer continued to enter water, floating parts started to adhere to the carrier wafer and be submerged in water. The adhering of parts is due to significant capillary forces introduced by trapped air bubbles between the parts and the carrier wafer (**Figure 24**). After all the floating parts adhered to the carrier wafer, the carrier wafer was withdrawn from water, and more than ~98% parts stayed attached. The final step to transfer these parts was to bring the carrier wafer approximately parallel to an alignment template on a 120 °C hotplate (**Figure 23(b)**), and these parts were then released to touch the alignment template with their pegs when water evaporated.

The next process step for the assembly sequence is to distribute the palletized silicon parts to an array of receptor sites on the alignment template. Orbital shaking was utilized to drive the parts to move until their pegs were trapped to receptor sites. Since orbital shaking provides a centrifugal force field, which is uniform in both magnitude and direction, and since the force direction is rotating in phase with the orbital shaker's rotating arms, parts are randomly moving locally instead of unidirectionally. Therefore, each unoccupied trap has an equal chance to have some parts to pass by, i.e., have a chance to trap the moving parts. Our trapping experiments with varying part redundancies gave yield–time curves shown in **Figure 25**.

The last process step was achieved by gravitationally driven self-alignment of anchored parts. When the alignment template was tilted in an appropriate orientation, gravitational forces drove the parts to rotate about their anchoring pegs to approach the equilibrium position with the lowest potential energies as a simple pendulum does (**Figure 26(a)** and **26(b)**). Kinetic frictional forces became smaller when the slope of the alignment template increased. Some parts can get stuck due to dust contamination or adsorbed moisture from the environment. A slight agitation at the edge of the alignment template (the impacting force must be in the plane of the alignment template) can break the sticking and free the parts to rotate. If the tilting orientation of the alignment template is precisely controlled, high accuracy of alignment can be achieved. Without good control of

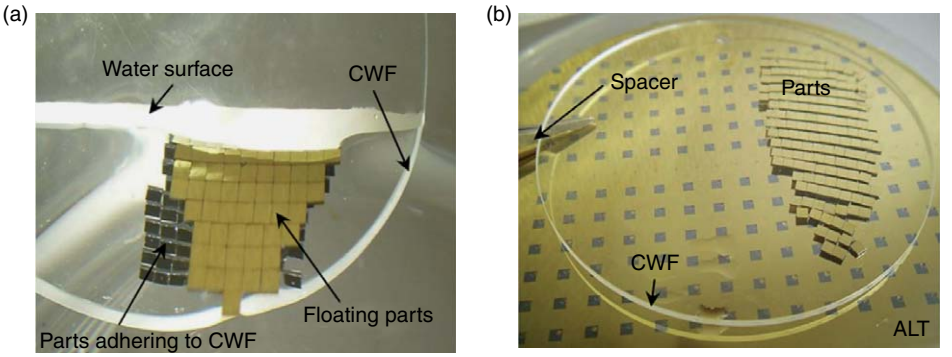

Figure 23 The palletizing process: (a) a carrier wafer inserted into water, and floating parts adhere to the hydrophobic PFC802 surface firmly; (b) the carrier wafer brought approximately parallel to an alignment template to release the adhering parts when water evaporates. (Source: Fang J, Böhringer K F 2005 High yield batch packaging of micro devices with uniquely orienting self-assembly. *Proc. IEEE Conf. Micro Electro Mechanical Systems*, Miami, FL, USA, pp. 12–15.)

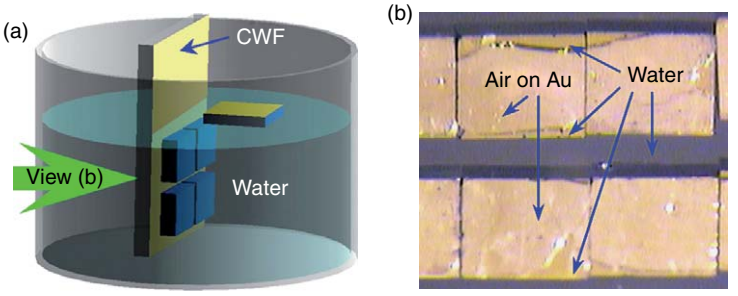

Figure 24 Mechanism of parts adhering to the hydrophobic surface: (a) a schematic view of a carrier wafer inserted vertically into water to pick up floating parts; (b) a microscopic image of trapped air bubbles underneath the parts adhering to the transparent carrier wafer in water. (Source: Fang J, Böhringer K F 2005 High yield batch packaging of micro devices with uniquely orienting self-assembly. *Proc. IEEE Conf. Micro Electro Mechanical Systems*, Miami, FL, USA, pp. 12–15.)

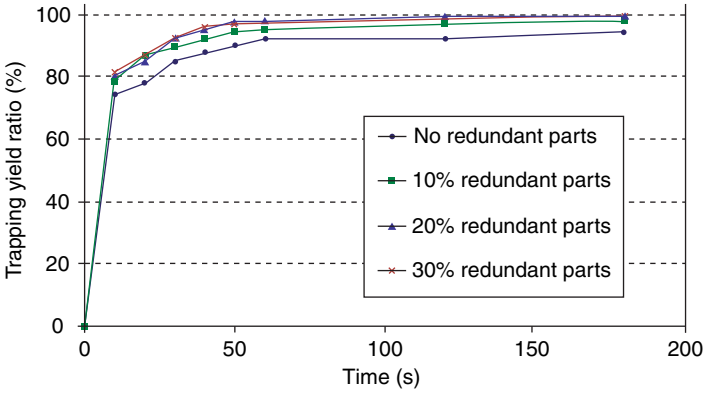

Figure 25 Trapping results of 2-mm square silicon parts on a 164 receptor site alignment template without and with 10–30% redundancy of parts. (Source: Fang J, Böhringer K F 2005 High yield batch packaging of micro devices with uniquely orienting self-assembly. *Proc. IEEE Conf. Micro Electro Mechanical Systems*, Miami, FL, USA, pp. 12–15.)

the template tilting, an additional wet fine alignment step was used: steam condensate was introduced into the parts and the template where steam formed film-wise and droplet-wise condensation on hydrophilic and hydrophobic surface areas, respectively. The receptor sites were hydrophilic with a hydrophobic background. The capillary gaps underneath the parts attracted steam condensation, so that parts self-aligned

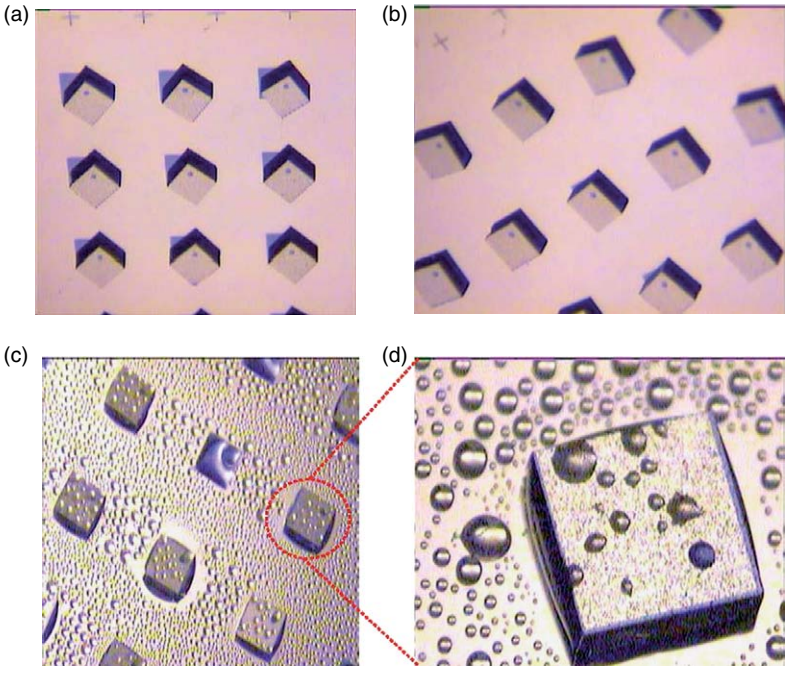

Figure 26 Uniquely aligning of 2-mm square silicon parts: (a) parts roughly aligned by gravity on a tilted alignment template; (b) parts roughly aligned to the receptor sites on an appropriately tilted alignment template; (c) misalignment corrected by capillary-driven self-alignment when water steam is introduced to condense on the alignment template and parts surface; and (d) a zoom view of a part with water condensate. (Source: Fang J, Böhringer K F 2005 High yield batch packaging of micro devices with uniquely orienting self-assembly. *Proc. IEEE Conf. Micro Electro Mechanical Systems*, Miami, FL, USA, pp. 12–15.)

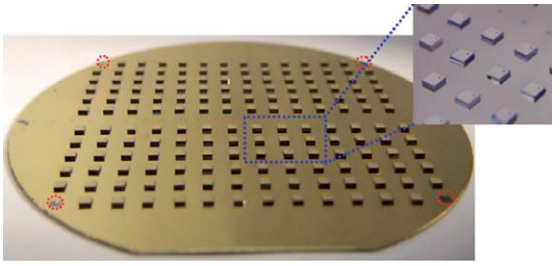

Figure 27 The assembly result: one hundred and sixty-four 2-mm square silicon parts correctly assembled on a 4″ alignment template (the four corner receptor sites were blocked by a covering petri dish to define moving range of the parts during the trapping experiment). (Source: Fang J, Böhringer K F 2005 High yield batch packaging of micro devices with uniquely orienting self-assembly. *Proc. IEEE Conf. Micro Electro Mechanical Systems*, Miami, FL, USA, pp. 12–15.)

to receptor sites by minimizing interfacial energies (**Figure 26(c)** and **26(d)**). After the parts were self-aligned, the water was evaporated by slow heating (rapid heating can cause nonuniform capillary stress on parts and can result in misalignment) to leave a dry aligned array of parts on the alignment template (**Figure 27**). At this stage, the aligned parts are ready to be transferred to a chip carrier template (CCT) via wafer-level flip chip bonding, and then dicing separates these simultaneously assembled or packaged devices.

1.14.3.7.2 Dry, uniquely orienting, self-organizing parallel assembly

To avoid aqueous assembly environments for microcomponents with released microstructures that can be easily immobilized or even broken by surface tension forces, Fang and Böhringer (2006b) developed a completely dry assembly process called DUO-SPASS. A schematic overview of this assembly process is shown in **Figure 28**. The main mechanism for this dry assembly is two-stage shape recognition: each part has one tall circular peg (CP) and one low cross peg (XP); each receptor site has correspondingly a circular trap (CT) and a cross trap (XT); the first stage assembly is achieved by anchoring a CP into a CT; the second stage assembly fixes the part in a specific in-plane orientation when its XP falls into an XT.

The pegs can be fabricated with either an additive or a subtractive method. A possible additive pattern

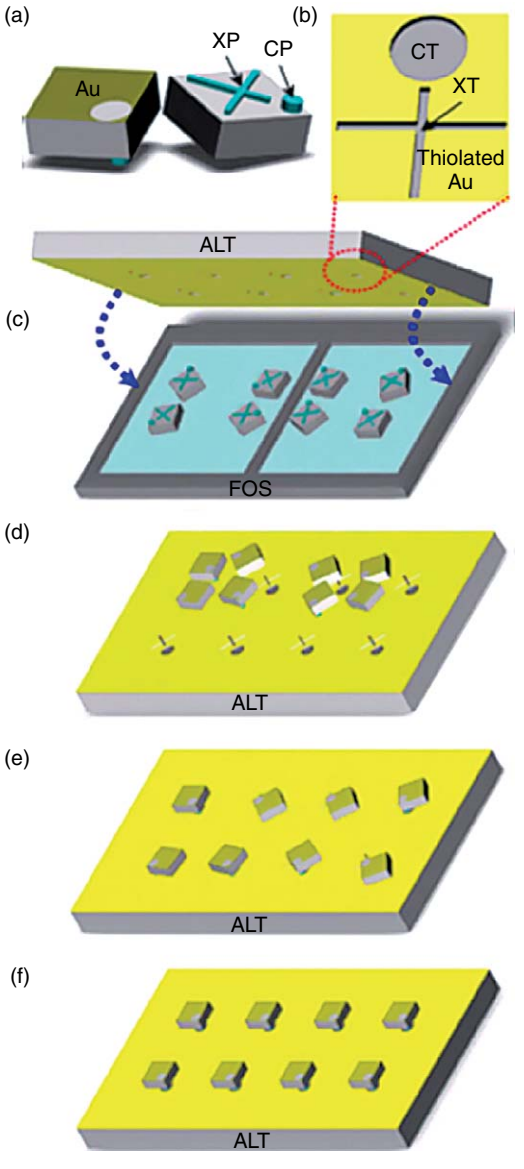

Figure 28 Schematic overview of the dry process to parallel assemble square microparts: (a) top and bottom views of a silicon part (the bottom face has a CP and an XP, and the CP has twice the height of the XP; the top face is coated with gold, and the opening in the gold layer marks the position of the CP); (b) trenches of a receptor site on the alignment template; (c) bulk parts face-oriented on an orbital shaken face-orienting substrate and then sandwiched by adding an alignment template; (d) parts palletized to the alignment template with their peg sides facing downward; (e) parts one-to-one anchored to receptor sites by orbital shaking: the CPs fall into the CTs (the first shape recognition); (f) parts rotated by orbital shaking introduce torques until their XPs fall into the XTs (the second shape recognition). (Source: Fang J, Böhringer K F 2006 Wafer-level packaging based on uniquely orienting self-assembly (the DUO-SPASS processes). *ASME/IEEE J. Microelectromech. Syst.* **15**, 531–40.)

method consists of double-layer SU8 casting (**Figure 29**), and a subtractive method is deep reactive ion etching (DRIE). The traps are fabricated with DRIE, with the depth of the traps being greater than that of the circular peg for stable anchoring.

A unique face orientation of bulk parts based on an asymmetry in dynamic stability was achieved. On an orbitally shaken plate, it is much more stable to rest bulk parts on their flat surfaces than on the pegs, and thus bulk parts are uniquely face-oriented to point upward with their pegs. Uniquely face-oriented parts are then transferred to an alignment template by the method shown in **Figure 28(c)** and **28(d)**.

Centrifugal forces generated by orbital shaking drive the parts to move until they are anchored to the circular traps (the first shape recognition). Since the anchored circular peg is located offset from the center of mass, a torque is exerted on each anchored part. The torque rotates each part until the second shape recognition is achieved: the cross peg falls into a cross trap. During this two-stage shape recognition, parts should move without flipping over, which can be achieved by the following:

(1) Lower orbital shaking speeds (~110 rpm for 1-mm square silicon parts)
(2) Thiolated gold coating on the alignment template for lower sliding friction
(3) An ultrasonic vibrating stage attached to the alignment template to reduce sticking effects and sliding friction.

Assembly results for 1-mm square silicon dummy parts are shown in **Figure 30**.

1.14.3.7.3 Parallel component-to-substrate assembly with controlled poses

Most of the reported parallel microassembly techniques had flat microcomponents assembled in only one pose: horizontal mounting on a substrate with the largest possible footprint. In some special cases, such as radio frequency MEMS (with MEMS = microelectromechanical system) and optical MEMS components, vertical mounting can benefit in the following ways:

(1) Less footprints and higher spatial density
(2) Functional surfaces (assuming to be the large flat surfaces) perpendicular to the assembly substrate.

Especially for VCSEL components, vertical mounting can direct a laser beam parallel to the substrate,

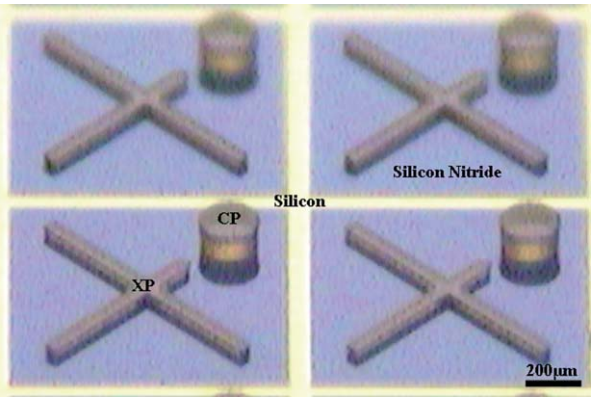

Figure 29 An optical microscope image of a 2 × 2 section of an array with SU8-2025 pegs on a 3″ silicon substrate, before dicing into individual parts. (Source: Fang J, Böhringer K F 2006 Wafer-level packaging based on uniquely orienting self-assembly (the DUO-SPASS processes). *ASME/IEEE J. Microelectromech. Syst.* **15**, 531–40.)

which enables the construction of free-space micro-optical systems and optical detectors for lab-on-chip microsystems.

A strategy to mount flat microcomponents parallelly on a substrate with either vertical or horizontal poses is shown schematically in **Figure 31**. Only a vertical pose is allowed for trapped components in the apertures due to geometrical constraints (**Figure 31(a)**). The surface tension of water is exploited to transfer the trapped vertically standing components onto a palletizing plate having an array of water-covered receptor sites (**Figure 31(b)** and **31(d)**). The transfer process leaves components vertically attached to the palletizing plate, i.e., components are assembled with vertical poses.

Assembly with a horizontal pose for a flat-edge component can be achieved by surface tension torques. The component has one hydrophobic surface, and the opposite surface is hydrophilic. After attaching to a water droplet, the component has more water on its hydrophilic face than does the other faces. The water droplets on the palletizing plate are formed by dip coating, and thus their volumes are limited by the dynamic contact angle of water and the receptor site area. For a 790 μm × 790 μm × 330 μm silicon component, the volume of a dip-coated water droplet cannot introduce enough surface tension torque on the hydrophilic surface to lay down the component. Steam condensation can introduce more water to increase the surface tension torque on the hydrophilic surface, and then the component will lie down on its hydrophilic surface as shown in **Figure 31(d)**. Optical images of an assembly process are shown in **Figure 32**.

1.14.4 Theoretical Aspects of Self-Assembly

The purpose of modeling, as discussed in this section, is twofold:

(1) To develop a theoretical understanding of the physical processes that are essential to self-assembly.
(2) To develop design tools that can help us to optimize engineered self-assembly processes and to establish the theoretical and practical bounds on their performance. The model presented here is very general. It simply assumes the existence of reaction rate constants that specify the speed at which components organize into aggregate structures, and assumes that this speed is proportional to the number of available parts and/or binding sites. Thus, it is applicable to all self-assembly approaches described in this review. However, the rate constants are highly dependent on the specific technique chosen, and they vary significantly with particular system parameters such as, for example, materials properties and scale of the components. Determining these rate constants can be achieved empirically by performing systematic sets of experiments. Alternatively, they can be derived from first principles; because of the complex interplay between the numerous effects that may influence a typical self-assembly process, such an *ab initio* approach remains a challenging task.

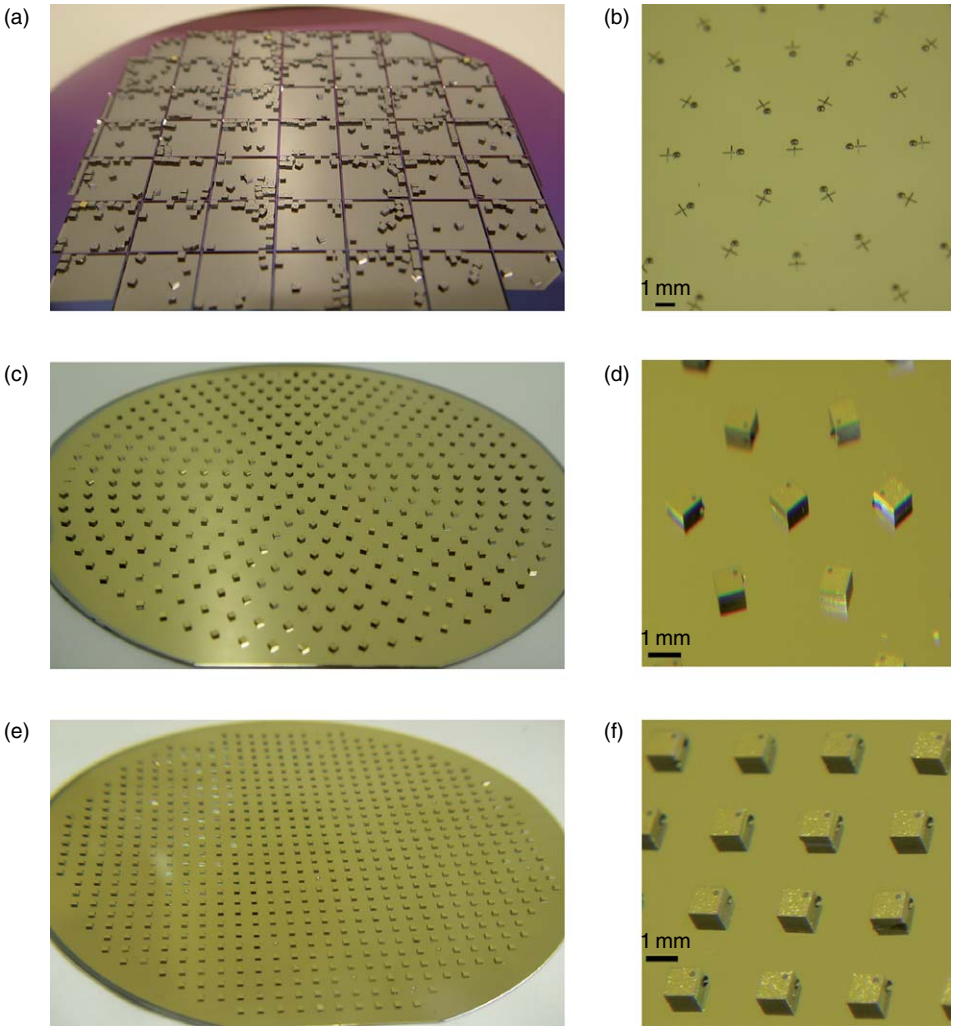

Figure 30 Optical photographs of templates and assembly results: (a) after 1 min of orbital shaking, almost all parts come to rest on their flat faces on the ϕ100-mm face-orienting substrate; (b) a partial view of an alignment template with a polar array of receptor sites; (c) 388 silicon parts assembled on the ϕ100-mm alignment template with a polar array of 397 receptor sites; (d) zoom-in view of the center of the alignment template; (e) 710 silicon parts assembled on the ϕ100-mm alignment template with an orthogonal array of 720 receptor sites; (f) zoom-in view of a 3×3 section of the array of receptor sites. (Source: Fang J, Böhringer K F 2006 Wafer-level packaging based on uniquely orienting self-assembly (the DUO-SPASS processes). *ASME/IEEE J. Microelectromech. Syst.* **15**, 531–40.)

1.14.4.1 Modeling

1.14.4.1.1 Parallels to chemical kinetics

A self-assembly process is, in principle, very similar to a chemical reaction. Typically, a large but finite number of reactants are available to interact and form bonds with each other. In chemistry, these reactants are atoms or molecules; in microscale self-assembly, they are, for example, silicon chips or hydrophobic binding sites. In either case, the reaction is of a stochastic nature and driven by energy minimization; however, the energy minimization for a microscale self-assembly relies on a wide range of possible sources, as described in Section 1.14.3. The equivalent of temperature is usually provided by some kind of mechanical agitation, such as the orbital shaker in the DUO-SPASS process described in Sections 1.14.3.7.1 and 1.14.3.7.2. Hosokawa *et al.* (1994) illustrated this connection to chemical kinetics with assemblies of tiles with moving permanent magnets that provided the binding force. A more detailed investigation followed in Cohn's (1997) Ph.D. thesis.

Whether or not a reaction takes place depends not only on the energy difference between the

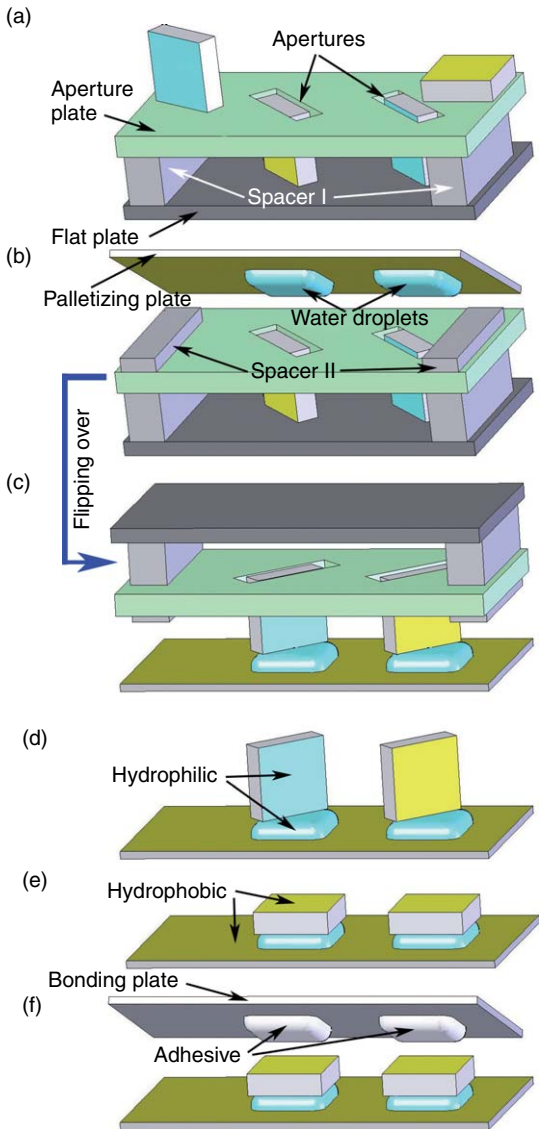

Figure 31 Schematic overview of the assembly process: (a) bulk parts fall into apertures vertically; (b) a palletizing plate carrying water droplets is aligned with the aperture plate; (c) the plates are flipped over to transfer parts on water droplets; (d) parts stand on receptor sites; (e) parts rotate to adhere to the palletizing plate with their hydrophilic oxide faces; (f) parts are permanently bonded to a bonding plate via wafer-level flip chip bonding. (Source: Fang J, Böhringer K F 2006 Parallel micro component-to-substrate assembly with controlled poses and high surface coverage. *IOP J. Micromech. Microeng.* **16**, 721–30.)

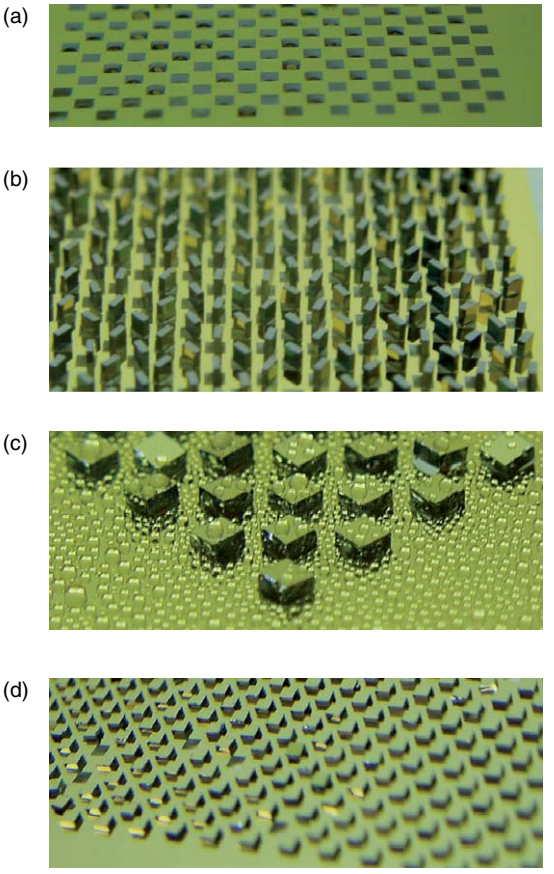

Figure 32 Optical images of 790-μm square parts transferred to a palletizing Pyrex plate via water droplets: (a) a partial view of an array of 790-μm square hydrophilic receptor sites covered with water droplets; (b) parts were transferred and are standing vertically; (c) water steam condensation was introduced on the palletizing plate, where steam formed filmwise and dropletwise condensation on hydrophilic and hydrophobic areas, respectively; (d) parts attached to receptor sites horizontally after steam condensation, with their only hydrophobic thiolated Au surface facing outward. (Source: Fang J, Böhringer K F 2006 Parallel micro component-to-substrate assembly with controlled poses and high surface coverage. *IOP J. Micromech. Microeng.* **16**, 721–30.)

unassembled and the assembled states, but also on the activation energy and the overall temperature of the system. Stiction between parts and substrates is a typical example of an energy barrier that has to be overcome either with careful engineering of the self-assembly system (e.g., nonstick hydrophobic surfaces and low humidity conditions) or with activation energy (e.g., vibration). This activation energy can be understood as the temperature of the system, and agitation with a piezoactuator or an orbital shaker is the analog of Brownian motion.

Consider the semi-DUO-SPASS self-assembly system described in Section 1.14.3.7.1 as an example. Here, gravity provides the potential energy difference that causes the parts to assemble in the cavities. If we have n binding sites and rn parts ($r \geq 1$ is the

part redundancy) we can initially expect a forward reaction rate of $K_f rn^2$, where K_f is the rate constant of the forward reaction. As parts are consumed and binding sites fill up, this rate changes to $K_f(rn-x)(n-x)$ with x being the number of already occupied sites. We can thus express x through a differential equation: $dx/dt = K_f(rn-x)(n-x)$. This equation has a closed-form solution

$$x(t) = \frac{rn(1-\exp(-K_f(r-1)nt))}{r-\exp(-K_f(r-1)nt)} \quad [1]$$

and x approaches 100% as t goes toward infinity. In Figure 33, the rate constant is set to $K_f = 1$ part per time unit and $r = 1.1$, 1.2, and 1.3.

In practice, 100% yield is difficult to achieve because (a) assembly has to be terminated in a finite – and usually short – amount of time and (b) there may also exist a nonzero reaction in the reverse direction that causes occasional breakup of already assembled parts. Let K_r be the rate constant for the reverse reaction, and we expect that usually $K_r < K_f$. Then eqn [1] needs to be updated to include the reverse reaction whose rate is $K_r x$. Note that here x is a linear term and not a quadratic term as in the forward reaction. This is due to the combinatorics of this particular self-assembly system, where the number of free part–free binding site combinations is quadratic in x but the number of occupied sites is linear in x. Thus we obtain a new differential equation $dx/dt = K_f(rn-x)(n-x) - K_r x$. This equation, again, can be solved exactly, and we can derive the equilibrium equation

$$x = \frac{K_{rf} + (r+1)n}{2} - \sqrt{\left(\frac{K_{rf} + (r+1)n}{2}\right)^2 - rn^2} \quad [2]$$

where K_{rf} stands for K_r/K_f. For $K_{rf} = 0.1$ and $r = 1.1$, 1.2, and 1.3, we now obtain equilibria at 97.0%, 98.2%, and 98.7%, respectively (Figure 34).

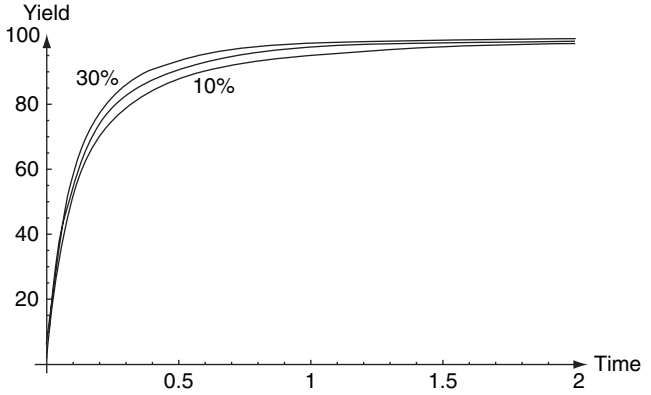

Figure 33 Theoretically determined yield of a self-assembly process described by eqn [1] as a function of time, with part redundancy at 10%, 20%, and 30%.

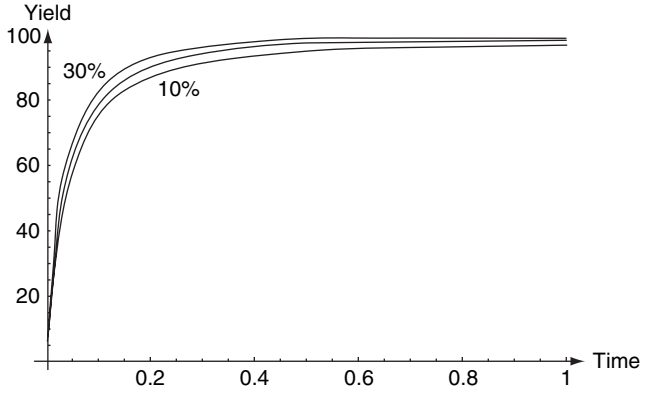

Figure 34 Theoretically determined yield of a self-assembly process that takes into account forward reaction rate $K_f = 1$ and reverse reaction rate $K_r = 0.1$. Again, part redundancy is 10%, 20%, and 30%. The self-assembly processes reach a yield of 97.0%, 98.2%, and 98.7%, respectively.

This analysis could be further refined in many ways. For example, note that eqns [1] and [2] assume a reaction-limited process. In practice, this means that parts are sufficiently mobile to reach all binding sites. If instead a diffusion-limited process is chosen (i.e., the parts' mobility is more constrained such that only parts in the immediate vicinity of a binding site can react) then the equation must be adjusted again. Another limitation of eqns [1] and [2] is the application of a continuous equation to a discrete system. Alternatively, one can express the assembly in terms of discrete states, and each reaction corresponds to a state transition. Such a system can be represented by a directed graph where each node represents a state and each edge a (probabilistic) transition. The theory of Markov processes provides a powerful and well-developed foundation for this approach.

1.14.4.1.2 Predicting and optimizing performance

When describing a self-assembly system, we can distinguish between process parameters and performance parameters. Process parameters describe the physical conditions under which the system operates: geometry, material properties, environmental conditions, part counts, etc. Performance parameters provide a metric to evaluate the self-assembly process: yield, assembly time, accuracy, wear on parts, etc.

The model equations in Section 1.14.4.1.1 indicate process parameters that influence specific performance parameters. If our objective is to maximize the number of assemblies x in a given time t, then intuitively we would choose a large part redundancy r and a large ratio between the rate constants K_f and K_r. The equations confirm this strategy but also give bounds on the yield, which we can expect from a practical experimental setup.

Calculating exact values for the rate constants K_f and K_r for self-assembly processes from first principles is difficult in general. The challenge lies in the usually complex interplay of different phenomena (gravity, capillarity, van der Waals forces, etc.) and in the difficulty to find the equivalent of temperature (i.e., kT) in reaction kinetics. Further research is needed in this area to establish a generally applicable theory of microscale self-assembly.

1.14.4.2 Parallels between Assembly and Computation

Another fascinating aspect of self-assembly is its close relationship to computation. Adleman's seminal paper showed that nondeterministic polynomial time (NP)-hard problems can be encoded into DNA molecules (Adleman 1994). Moreover, it is well-known that self-assembly systems consisting of simple 2D tiles can implement a Turing machine, and thus can perform (in principle) any computation (Grünbaum and Shephard 1986, Wang 1963). This result may not lead to practical computers based on self-assembly, but it indicates that virtually arbitrarily complex structures could be created via self-assembly, given a sufficiently sophisticated program that guides the assembly toward the desired product. Real-time error correction is essential because, as we have seen throughout Section 1.14.3, stochastic processes cannot be expected to produce perfect yield. To date, biological growth in nature remains by far the best proof of principle for successful self-assembly.

1.14.5 Discussion and Outlook

Self-assembly techniques enable rapid and parallel construction processes for MEMS devices. With appropriate driving forces, self-assembly techniques can assemble components ranging from submicrons to millimeters or larger scales, while conventional robotic pick-and-place assembly methods face mounting difficulties below 500 μm due to sticking effects between grippers and components. The following research directions are worthy of efforts to further extend the capabilities of self-assembly techniques.

In the previous sections, several major self-assembly techniques driven by inertial, electrical, magnetic, and interfacial energy minimization have been discussed. Each of these self-assembly techniques can achieve both 2D and 3D assemblies with appropriate structure designs. Current and potential applications of these self-assembly techniques are given in **Table 1**.

Three-dimensional self-assembly methods will most likely play a key role in building MEMS devices with more complicated architectures. Most of the currently available self-assembly techniques mount microcomponents on a substrate surface, i.e., a 2D assembly process. To achieve multiple functions or stand-alone applications, a MEMS device can be integrated with various components such as MEMS sensing units, MEMS actuating units, or complementary metal oxide semiconductor (CMOS) signal processing units. Three-dimensional assembly

Table 1 Current and potential applications of each self-assembly technique

Inertial	2D	• Mass fabrication of RFID tags by fluidic self-assembly • Self-assembly of microcomponents by single- or double-stage shape recognition
	3D	• Construction of 3D structures by centrifugal forces driving hinged structures • Potential construction of 3D structures by feature mating
Interfacial	2D	• Patterning and aligning of microcomponents on a substrate by capillary forces of melting solder or other liquids
	3D	• Integration of different types of microcomponents to form a hybrid composite component • Construction of 3D structures by reflowing solder or photoresist deposited at hinges
Electrical	2D	• Patterning of micro- and nanoscale components on a substrate • Programmable assembly of hybrid components
	3D	• Construction of 3D structures by triboelectricity • Potential aligning of nanowires in desired orientations
Magnetic	2D	• Integration of semiconductor components to recessed sites with magnetized strips on a substrate • Potential programmable assembly of heterogeneous components
	3D	• Construction of 3D frames by sequential pricking up of hinged structures • Potential building of 3D structures by attaching components of specific geometric design

enables dense packaging of these components, which can greatly reduce environmental disturbances and signal transmission losses among different functional units.

Assembly programmability will greatly widen the application range of self-assembly techniques and enable construction of more versatile MEMS devices. This programmability can indicate several situations such as the following:

(1) Integration of different types of components by multiple batches of self-assembly
(2) Self-assembly of same types of components into various patterns in different batches
(3) Selective disassembly of some components by breaking up their bonds to receptor sites
(4) Assembly of multiple components in appropriate sequences to form 3D structures

A consequence of the stochastic nature of self-assembly is that in most cases, perfect yields of 100% cannot be expected. As a remedy, redundancy could be incorporated into the assembly, for example, by including more than the minimum required amount of components. Intentional disassembly of incorrectly placed components is also a possibility, but it would require binding sites that can be deactivated even after assembly has already taken place. Finally, a precision robotic assembly step could also be employed to place any remaining defects.

Assembly process automation enables running the self-assembly process continuously for maximum throughput. To this end, one needs to consider how the process can be integrated into the overall production flow, including parts feeding, redundant parts recycling, assembly defect recognition, and recovery. The high capital investment and specialized equipment used in prior and subsequent processing steps should not be affected by the introduction of a new process step. Thus, ideally, the inputs and outputs of the self-assembly process module should be identical with the conventional assembly module that it replaces. This may imply additional constraints on how the substrate and parts are delivered to and from the self-assembly module.

Acknowledgments

The authors would like to thank Kerwin Wang, Xiaorong Xiong, Yanbing Wang and Sheng-Hsiung Liang in the MEMS research group of the University of Washington, Rajashree Baskaran at Intel Corporation, Vaidyanathan Kripesh and his team at A*STAR IME for helpful comments and discussions. This work was supported in part by NSF award ECS-05-1628, NIH Center of Excellence in Genomic Science and Technology grant 1-P50-HG002360-01, DARPA DSO award FAA9550-04-0257, and US Department of Justice award 2000-DT-CX-K001.

References

Adleman L 1994 Molecular computation of solutions to combinatorial problems. *Science* **266**, 1021–4

Böhringer K F, Goldberg K, Cohn M, Howe R T, Pisano A 1998 Parallel microassembly with electrostatic force fields. *Proc. Int. Conf. Robotics and Automation (ICRA)*, Leuven, Belgium, pp. 1204–11

Böhringer K F, Srinivasan U, Howe R T 2001 Modeling of fluidic forces and binding sites for fluidic self-assembly. *Proc. IEEE Int. Conf. Micro Electro Mechanical Systems (MEMS)*, Interlaken, Switzerland, pp. 369–74

Cohn M 1997 Assembly techniques for microelectromechanical systems. Electrical Engineering and Computer Sciences. Ph.D. thesis, University of California

Cohn M B, Howe R T, Pisano A P 1995 Self-assembly of microsystems using non-contact electrostatic traps. *Proc. ASME Int. Cong. Exposition, Symp. Micromechanical Systems, (IC '95)*, San Francisco, CA, USA, pp. 893–900

Fang J, Böhringer K F 2005 High yield batch packaging of micro devices with uniquely orienting self-assembly. *Proc. IEEE Int. Conf. Micro Electro Mechanical Systems (MEMS)*, Miami, FL, USA, pp. 12–15

Fang J, Böhringer K F 2006a Parallel micro component-to-substrate assembly with controlled poses and high surface coverage. *IOP J. Micromech. Microeng.* **16**, 721–30

Fang J, Böhringer K F 2006b Wafer-level packaging based on uniquely orienting self-assembly (the DUO-SPASS processes). *ASME/IEEE J. Microelectromech. Syst.* **15**, 531–40

Fang J, Wang K, Böhringer K F 2006 Self-assembly of PZT actuators for micro pumps with high process repeatability. *ASME/IEEE J. Microelectromech. Syst.* **15**, 871–8

Fearing R S 1995 A planar milli-robot on an air bearing. *Proc. Int. Symp. Robotics Research*, Herrsching, Germany, pp. 570–81

Gracias D H, Tien J, Breen T L, Hsu C, Whitesides G M 2000 Forming electrical networks in three dimensions by self-assembly. *Science* **289**, 1170–2

Grünbaum B, Shephard G C 1986 *Tilings and Patterns*. Freeman, New York

Harsh K F, Kladitis P E, Zhang Y H, Dunn M L, Bright V M, Lee Y C 2000 Tolerance and precision study for solder self-assembled MEMS. *Proc. SPIE* **4075**, 173–84

Hosokawa K, Shimoyama I, Miura H 1994 Dynamics of self-assembling systems – Analogy with chemical kinetics. *Artif. Life* **1**, 413–27

Iwase E, Shimoyama I 2005 Multi-step sequential batch self-assembly of three-dimensional micro-structures using magnetic field. *Proc. IEEE Int. Conf. Micro Electromechanical Systems (MEMS)*, Miami Beach, FL, USA, pp. 588–91

Jacobs H O, Tao A R, Schwartz A, Gracias D H, Whitesides G M 2002 Fabrication of cylindrical display by patterned assembly. *Science* **296**, 323–5

Kaajakari V, Lal A 2001 Electrostatic batch assembly of surface MEMS using ultrasonic triboelectricity. *14th IEEE Int. Conf. Micro Electro Mechanical Systems (MEMS)*, Interlaken, Switzerland, pp. 10–13

Kladitis P E, Bright V M 2000 Prototype microrobots for micro-positioning and micro-unmanned vehicles. *Sens. Actuators* **A80**, 132–7

Lai K W C, Hui A P, Li W J 2002 Non-contact batch micro-assembly by centrifugal force. *Proc. IEEE Int. Conf. Micro Electro Mechanical System (MEMS)*, Las Vegas, NV, pp. 184–7

Liang S, Xiong X, Böhringer K F 2004 Towards optimal designs for self-alignment in surface-tension driven micro-assembly. *Proc. IEEE Int. Conf. Micro Electro Mechanical Systems (MEMS)*, Maastricht, The Netherlands, pp. 9–12

Liang S, Wang K, Böhringer K F 2005 Self-assembly of MEMS components in air assisted by diaphragm agitation. *Proc. IEEE Conf. Int. Micro Electro Mechanical Systems (MEMS)*, Miami Beach, FL, USA, pp. 592–5

Perkins J, Rumpler J, Fonstad C G 2002 Magnetically assisted self-assembly – A new heterogeneous integration technique. *MIT Microsystems Technology Laboratories Annual Report*

Silicon Chip Online 2006 *RFID tags – How they work*. http://www.siliconchip.com.au/cms/A_30750/article.html

Skidmore G D, Ellis M, Parker E, Sarkar N, Merkle R 2000 Micro-assembly for top-down nanotechnology. *Proc. Int. Symp. Micromechatronics and Human Science*, Nagoya, Japan, pp. 3–9

Srinivasan U, Liepmann D, Howe R T 2001 Microstructure to substrate self-assembly using capillary forces. *J. Microelectromech. Syst.* **10**, 17–24

Stauth S A, Parviz B A 2005 Self-assembled silicon networks on plastic. *Proc. 13th Int. Conf. Solid-State Sensors and Actuators,* Vol. 1, pp. 964–7

Syms R R A, Yeatman E M, Bright V M, Whitesides G M 2003 Surface tension-powered self-assembly of microstructures – The state-of-the-art. *IEEE J. Microelectromech. Syst.* **12**, 387–417

Tien J, Terfort A, Whitesides G M 1997 Microfabrication through electrostatic self-assembly. *Langmiur* **13**, 5349–55

Wang H 1963 *Proc. Symp. Math. Theory of Automata,* New York, NY, USA

Warneke B, Last M, Liebowitz B, Pister K S J 2001 Smart Dust: Communicating with a cubic-millimeter computer. *Computer* **34**, 44–51

Xiong X, Hanein Y, Fang J, Wang Y, Wang W, Schwartz D T, Böhringer K F 2003 Controlled multi-batch self-assembly of micro devices. *IEEE J. Microelectromech. Syst.* **12**, 117–27

Yang H, Lin C, Fang W 2006 Wafer level self-assembly of microstructures using global magnetic lifting and localized induction welding. *IOP J. Micromech. Microeng.* **16**, 27–32

Yeh H J, Smith J S 1994 Fluidic self-assembly for the integration of GaAs light-emitting diodes on Si substrates. *IEEE Photonics Technol. Lett.* **6**, 706–8

Zheng W, Buhlmann P, Jacobs H O 2004 Sequential shape-and-solder-directed self-assembly of functional microsystems. *Proc. Natl. Acad. Sci. USA* **101**, 12814–17

Biographies

Jiandong Fang received his Bachelor's degree in Physics from the University of Science and Technology of China in 1999 and his Master's degree in Physics and the Ph.D. degree in Electrical Engineering from the University of Washington (Seattle, WA) in 2001 and 2006, respectively. From September 2006, he worked as a postdoc research fellow at the School of Electrical and Computer Engineering, Georgia Institute of Technology, Atlanta, GA.

His current research is mainly focused on self-assembly of microcomponents, design, fabrication, and packaging of microelectromechanical systems (MEMS) such as fluidic pumps, scanning mirrors, biochemical sensors, and piezoelectrically driven MEMS resonators.

Karl F. Böhringer received his Dipl.-Inform. degree from the University of Karlsruhe, Germany, in 1990 and his MS/Ph.D. degrees in Computer Science from Cornell University, Ithaca, NY, in 1993/1997.

He was a Visiting Scholar at Stanford University in 1994–1995 and a Postdoctoral Researcher at the University of California, Berkeley from 1996 to 1998. He joined the Electrical Engineering department at the University of Washington in Seattle, WA, in 1998, where he is currently Associate Professor. He also held visiting faculty positions at the Universities of Tohoku, Tokyo, Kyoto (Japan), and São Paulo (Brazil). His research interests include microelectromechanical systems (MEMS), manipulation and assembly from macro- to nanoscales, microfluidic systems for the life sciences, and microrobotics. He has created, among others, multibatch self-assembling systems, massively parallel microactuator arrays, and a walking microrobot.

Karl F. Böhringer is a member of the Society for Nanoscale Science, Computing and Engineering (ISNSCE), the American Society for Engineering Education (ASEE), and the German Society for Information Sciences (GI). He was awarded a Long-Term Invitational Fellowship for Research in Japan by the Japan Society for the Promotion of Science (JSPS) in 2004, an IEEE Robotics & Automation Society Academic Early Career Award in 2004, an NSF CAREER Award in 1999, and an NSF Postdoctoral Associateship in 1997. His work was listed among the Top 100 Science Stories of 2002 in *Discover* magazine. He is an associate editor of ASME/IEEE Journal of Microelectromechanical Systems and IEEE Transactions on Automation Science and Engineering and has served, among others, on technical program committees for the IEEE MEMS and Transducers conferences.